



## OPEN ACCESS

## EDITED BY

Jose Martin Hernandez-Ayon,  
Autonomous University of Baja California,  
Mexico

## REVIEWED BY

Carla F. Berghoff,  
Instituto Nacional de Investigación y  
Desarrollo Pesquero, Argentina  
Luz De Lourdes Aurora Coronado Alvarez,  
Autonomous University of Baja California,  
Mexico

## \*CORRESPONDENCE

Carlos Augusto Musetti de Assis  
[✉ cmusetti@geomar.de](mailto:cmusetti@geomar.de)

RECEIVED 31 August 2023

ACCEPTED 24 May 2024

PUBLISHED 01 July 2024

## CITATION

Musetti de Assis CA, Pinho LQ, Fernandes AM,  
Araujo M and Cotrim da Cunha L (2024)  
Reconstruction of the marine carbonate  
system at the Western Tropical Atlantic:  
trends and variabilities from 20 years  
of the PIRATA program.  
*Front. Mar. Sci.* 11:1286960.  
doi: 10.3389/fmars.2024.1286960

## COPYRIGHT

© 2024 Musetti de Assis, Pinho, Fernandes,  
Araujo and Cotrim da Cunha. This is an open-  
access article distributed under the terms of  
the [Creative Commons Attribution License  
\(CC BY\)](https://creativecommons.org/licenses/by/4.0/). The use, distribution or reproduction  
in other forums is permitted, provided the  
original author(s) and the copyright owner(s)  
are credited and that the original publication  
in this journal is cited, in accordance with  
accepted academic practice. No use,  
distribution or reproduction is permitted  
which does not comply with these terms.

# Reconstruction of the marine carbonate system at the Western Tropical Atlantic: trends and variabilities from 20 years of the PIRATA program

Carlos Augusto Musetti de Assis<sup>1,2,3\*</sup>, Luana Queiroz Pinho<sup>1,2</sup>,  
Alexandre Macedo Fernandes<sup>1</sup>, Moacyr Araujo<sup>2,4,5</sup>  
and Leticia Cotrim da Cunha<sup>1,2,5</sup>

<sup>1</sup>Programa de Pós-Graduação em Oceanografia, Laboratório de Oceanografia Química, Universidade do Estado do Rio de Janeiro (UERJ), Rio de Janeiro, RJ, Brazil, <sup>2</sup>Brazilian Ocean Acidification Network (BrOA), Universidade Federal do Rio Grande (FURG), Rio Grande, RS, Brazil, <sup>3</sup>GEOMAR Helmholtz Centre for Ocean Research Kiel, Kiel, Germany, <sup>4</sup>Departamento de Oceanografia, DOCEAN/Universidade federal de Pernambuco (UFPE), Recife, Brazil, <sup>5</sup>Brazilian Research Network on Global Climate Change (Rede CLIMA), São José dos Campos, SP, Brazil

The Western Tropical Atlantic Ocean (WTAO) is crucial for understanding CO<sub>2</sub> dynamics due to inputs from major rivers (Amazon and Orinoco), substantial rainfall from the Intertropical Convergence Zone (ITCZ), and CO<sub>2</sub>-rich waters from equatorial upwelling. This study, spanning 1998 to 2018, utilized sea surface temperature (SST) and sea surface salinity (SSS) data from the PIRATA buoy at 8°N 38°W to reconstruct the surface marine carbonate system. Empirical models derived total alkalinity (TA) and dissolved inorganic carbon (DIC) from SSS, with subsequent estimation of pH and fCO<sub>2</sub> from TA, DIC, SSS, and SST data. Linear trend analysis showed statistically significant temporal trends: DIC and fCO<sub>2</sub> increased at a rate of 0.7 μmol kg<sup>-1</sup> year<sup>-1</sup> and 1.539 μatm year<sup>-1</sup>, respectively, and pH decreased at a rate of -0.001 pH units year<sup>-1</sup>, although DIC did not show any trend after data was de-seasoned. Rainfall analysis revealed distinct dry (July to December) and wet (January to June) seasons, aligning with lower and higher freshwater influence on the ocean surface, respectively. TA, DIC, and pH correlated positively with SSS, exhibiting higher values during the dry season and lower values during the wet season. Conversely, fCO<sub>2</sub> correlated positively with SST, showcasing higher values during the wet season and lower values during the dry season. This emphasizes the influential roles of SSS and SST variability in CO<sub>2</sub> solubility within the region. Finally, we have analysed the difference between TA and DIC (TA-DIC) as an indicator for ocean acidification and found a decreasing trend of  $-0.93 \pm 0.02$  μmol kg<sup>-1</sup> year<sup>-1</sup>, reinforcing the reduction in the surface ocean buffering capacity in this area. All trends found for the region agree with data from other stations in the tropical and subtropical Atlantic Ocean. In conclusion, the use of empirical models proposed in this study has proven to help filling the gaps in marine carbonate system data in the Western Tropical Atlantic.

## KEYWORDS

ocean acidification, pH, CO<sub>2</sub>, time series, total alkalinity, dissolved inorganic carbon

## 1 Introduction

With the advance of human civilization in the past decades came the increase of carbon dioxide (CO<sub>2</sub>) emissions in the atmosphere due to the burning of fossil fuels, the main present source of energy (Mardani et al., 2019). This is one of the greenhouse gases responsible for keeping the global temperature steady. Nonetheless, the rise of CO<sub>2</sub> emissions has been leading to global changes such as global atmosphere and ocean warming, a decrease in seawater pH, as well as an increase of extreme climatic events' frequency (Allen et al., 2009; Doney et al., 2009; Baker et al., 2018).

The global ocean serves as a significant CO<sub>2</sub> sink, absorbing approximately 25% of annual human emissions (Sabine et al., 2004; Friedlingstein et al., 2022). Carbon dioxide's solubility at the sea surface depends primarily on sea surface temperature (SST) and sea surface salinity (SSS), rendering the global ocean a complex, dynamic system intricately linked to the atmosphere (Goodwin and Lenton, 2009; Takahashi et al., 2009; Merlivat et al., 2015). When CO<sub>2</sub> reacts with water, it forms carbonic acid (H<sub>2</sub>CO<sub>3</sub>), releasing protons (H<sup>+</sup>) and bicarbonate ions (HCO<sub>3</sub><sup>-</sup>). The increase in the CO<sub>2</sub> absorption results in a reduction of carbonate saturation, effect known as ocean acidification, affecting organisms with calcified structures, as illustrated in Equation 1 (Guinotte and Fabry, 2008; Pörtner, 2008; Kroeker et al., 2010; Mangi et al., 2018; Bednaršek et al., 2019). This phenomenon has various impacts on marine life, including hindering the formation of calcareous structures, reducing recruitment rates of organisms on coral reefs, and intensifying competition between non-calcifying and calcifying organisms (Bignami et al., 2013; Allen et al., 2017).

Biological processes significantly influence CO<sub>2</sub> dynamics in the ocean. Intense primary production consumes dissolved CO<sub>2</sub>, elevating seawater pH. Conversely, when respiration surpasses primary production, CO<sub>2</sub> is added to the water, causing a pH decline (Sunda and Cai, 2012; Buapet et al., 2013). Notably, this impact is more pronounced in coastal regions and oceanic areas experiencing intense upwelling (Dugdale et al., 2002; McGillis et al., 2004; Wallace et al., 2014).



The reactions involve essential components of the marine carbonate system: total alkalinity (TA), dissolved inorganic carbon (DIC), pH, and CO<sub>2</sub> fugacity (*f*CO<sub>2</sub>). TA represents the surplus of proton acceptor species in seawater, primarily carbonate and bicarbonate ions at a pH of 8.1. Contributions from the boric system and water dissociation components are considered (Dickson, 1981; Wolf-Gladrow et al., 2007; Emerson and Hedges, 2008; Doney et al., 2009).

DIC comprises dissolved CO<sub>2</sub>, carbonic acid (H<sub>2</sub>CO<sub>3</sub>), bicarbonate, and carbonate ions, representing the summation of all inorganic carbon species in seawater (Emerson and Hedges, 2008). The pH scale measures seawater acidity and can be represented in various scales, defined as the negative logarithm (base 10) of the H<sup>+</sup> ion concentration, indicating water acidity levels (Marion et al., 2011). *f*CO<sub>2</sub> corrects the partial pressure of CO<sub>2</sub>

(*p*CO<sub>2</sub>) from an ideal to a real gas, representing the gas pressure exerted within the water (Dickson et al., 2007).

Any two of the marine carbonate system parameters, together with SSS and sea surface temperature (SST) values, can be used to calculate the remaining parameters (Schneider et al., 2007; Fassbender et al., 2017). Empirical models correlating TA and DIC with sea surface salinity (SSS) have a great importance in comprehending the marine carbonate system as they can be used in historic series for reconstructing past data (Lee et al., 2006; Lefèvre et al., 2010; Bonou et al., 2016). Most of the carbonate system parameters of this system were not usually measured in the past, meaning that calculating them from SSS data is a good alternative when these empirical models are well established for the study area.

The tropical Atlantic (30°S-30°N; 80°W-20°E) acts on average as a source of CO<sub>2</sub> to the atmosphere, mainly because of higher temperatures decreasing the gas solubility, as well as the equatorial upwelling bringing CO<sub>2</sub>-rich subsurface water and increasing the CO<sub>2</sub> fugacity at the ocean surface (Takahashi et al., 2009; Schuster et al., 2013). However, the Western Tropical Atlantic Ocean (WTA) goes the other way around, becoming a large sink of atmospheric CO<sub>2</sub> at the Tropical Atlantic from July to December, in response to large inputs of freshwater, both from the Intertropical Convergence Zone's (ITCZ) rainfall and from the Amazon River plume. During that period, Amazon waters widely spread to the western parts of the WTA after the North Brazilian Current (NBC) retroreflection and eastward transport by North Equatorial Countercurrent (NECC) (Mitchell and Wallace, 1992; Körtzinger, 2003; Bruto et al., 2017; Lefèvre et al., 2017).

Time series are of great importance in the study of trends and variability in the marine carbonate system. Bates et al. (2014) observed a trend in DIC, pH, *p*CO<sub>2</sub> and other parameters in this system from time series with 15 to 30 years in five stations in the Atlantic Ocean and two stations in the Pacific, elucidating how different parts of the global ocean responded to the increase in atmospheric concentrations of CO<sub>2</sub>, as well as to ocean acidification.

The PIRATA project, initiated in 1997, aims to understand Tropical Atlantic Ocean variability. Using 18 moored buoys, it forms a real-time observation network to monitor meteorological and oceanographic variables (Bourlès et al., 2019; Foltz et al., 2019). This multinational effort enhances our ability to predict ocean-atmosphere variability. Moored buoys are crucial for capturing temporal variations in oceanographic parameters in the open ocean (Lefèvre et al., 2008; Bruto et al., 2017). Bruto et al. (2017) used the time series of hourly surface ocean *f*CO<sub>2</sub> data from the PIRATA buoy at 8° N 38° W, the same used in this study, from 2008 to 2011, where it was observed that, in addition to two distinct seasonal periods, *f*CO<sub>2</sub> also showed a high-frequency variation (less than 24h) associated with the daily cycle of solar radiation and heavy rainfall.

The WTA has been the focus of studies about the carbon cycle because of its great complexity and global importance concerning CO<sub>2</sub> dynamics (Araujo et al., 2017; Bonou et al., 2022, 2016; Lefèvre et al., 2017; de Carvalho-Borges et al., 2018; Monteiro et al., 2022). Although many studies show the spatial variation of the carbonate system on the WTA and its relationship with the Amazon River plume, few studies focus on analyzing its variation over longer

periods of time from *in situ* observations. This study used a time series from 1998 to 2018 of SSS and SST data from the PIRATA buoy at 8° N 38° W and calculated the carbonate system parameters (TA, DIC, pH and  $f\text{CO}_2$ ) to detect these parameters' variation with time in a region with complex  $\text{CO}_2$  dynamics.

## 2 Materials and methods

### 2.1 Data

The “Prediction and Research moored Array in the Tropical Atlantic” (PIRATA) project consists of an *in-situ* observation network composed of 18 moored buoys judiciously spread in the Tropical Atlantic. These include five buoys located along the 38°W meridian (4°N, 8°N, 12°N, 15°N, and 20°N). Each of these buoys are equipped with meteorological sensors to measure the direction and speed of the wind at 4 meters height, air temperature, rain rate, relative humidity and short-wave solar radiation. Temperature sensors are positioned beneath the ocean surface at depths of 1, 20, 40, 80, 120, 180, 300, and 500 meters, collecting measurements every 10 minutes. Salinity sensors are also deployed at depths of 1, 20, 40, and 120 meters, recording hourly measurements. The 8°N 38°W buoy data was considered in our study because: (i) it represents the PIRATA site under the strong seasonal influence of the Amazon River plume waters transported eastward by NECC and rainfall from the ITCZ; and (ii) a CARbon Interface Ocean Atmosphere (CARIOCA) sensor was installed on that mooring line from 2008–2013, registering *in situ* seawater  $f\text{CO}_2$  hourly values (Bruto et al., 2017). For this study, SSS and SST, both at 1m depth, and rain rate

data from the buoy located at 8°N 38°W were used (Figure 1) with a total of 3789 SSS and 5669 SST data. The daily averaged sea surface temperature (SST) and sea surface salinity (SSS) values are transmitted in real time by the Global Telecommunication System (GTS) and are freely available at PIRATA sites (e.g., <http://www.pmel.noaa.gov/pirata>) (Supplementary Material 1).

The SST and SSS data used in this study, from 1998 to 2018, were measured by the following sensors: a thermistor model 46006 from Yellow Springs Instruments (YSI) for measuring SST, with resolution of 0.001°C, range from 14 to 32°C and accuracy of  $\pm 0.03^\circ\text{C}$  (A'Hearn et al., 2002; Freitag et al., 2005), and, for the measurement of SSS, internal field conductivity cell of model SBE16 (Seacat) from Sea Bird Electronics with 0.0001  $\text{S m}^{-1}$  resolution, range from 3 to 6  $\text{S m}^{-1}$  and accuracy of  $\pm 0.02$  psu (Freitag et al., 1999). The lack of SSS data in relation to SST in the PIRATA buoy at 8°N 38°W is especially striking in the period from 2003 to 2008. As of 2010, both the available SSS and SST data decreased considerably due to vandalism and problems with the buoy's operation and maintenance. The rain rate data used to differentiate the two seasons in the time series were measured by a capacitance sensor from R. M. Young, model 50203–34, with resolution of 0.2  $\text{mm h}^{-1}$ , range from 0 to 50  $\text{mm h}^{-1}$  and accuracy of  $\pm 0.4$   $\text{mm h}^{-1}$  on 10 min filtered data (Serra et al., 2001). The PIRATA project conducts annual cruises dedicated to the retrieval of buoys and the maintenance of equipment. These cruises are essential for ensuring the continued functionality and reliability of the project's monitoring infrastructure. The data used in this study followed the World Ocean Circulation Experiment (WOCE) quality flag system (Gouretski and Koltermann, 2004), using Quality Flag (QF) 2 for valid data and 5 for missing data.

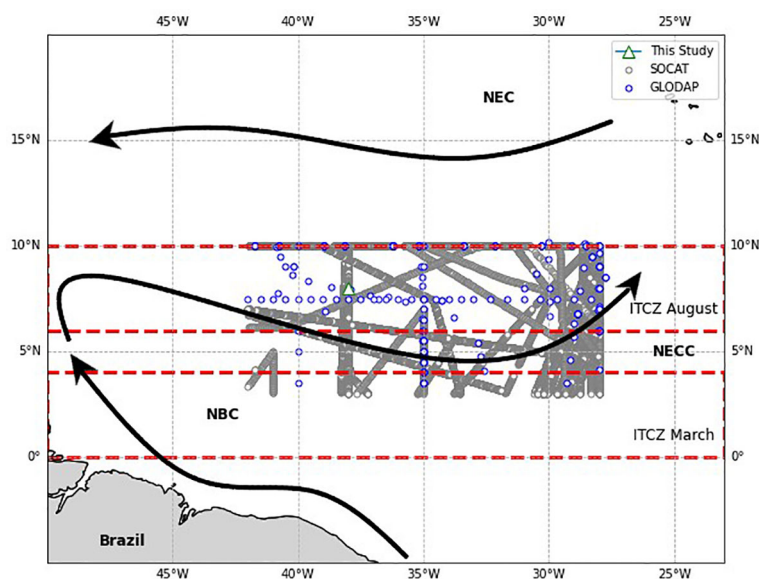


FIGURE 1

Study area. The green triangle represents the PIRATA mooring site at 8°N 38°W used in this study. The blue dots illustrate points where TA, DIC and pH data from GLODAPv2.2022 were used. The main surface currents are also shown on the map, together with the mean position of the Intertropical Convergence Zone (ITCZ) at its southernmost (March) and northernmost (August) months. NEC, North Equatorial Current; NECC, North Equatorial Countercurrent; NBC, North Brazilian Current.

## 2.2 Calculation of parameters

In this study, the calculation of TA relied on the equation proposed by Lefèvre et al. (2010) (Equation 2), which correlates TA with SSS in the Western Tropical Atlantic. It's important to note the associated error of  $11.6 \mu\text{mol kg}^{-1}$  in predicted alkalinity using this equation. Similarly, for DIC, the equation proposed by Bonou et al. (2016) was employed (Equation 3), presenting an error of  $24 \mu\text{mol kg}^{-1}$  in predicted DIC. Additionally, an annual increase of  $0.9 \mu\text{mol kg}^{-1}$  in DIC since 1989 was factored in to account for the escalating annual  $\text{CO}_2$  emissions into the atmosphere. As detailed by Bonou et al. (2016), the inclusion of SST data in these regression equations did not significantly enhance correlation, indicating that SSS variations exerted a more substantial influence on TA and DIC variability in the Western Tropical Atlantic compared to SST. The uncertainties of these estimations were thoroughly discussed by the authors before mentioned, highlighting the importance of regionally using these equations, as they are strongly related to the local SSS variation observed in the WTA.

$$TA = 58.1 (\pm 0.5) * SSS + 265 (\pm 18) \quad R^2 = 0.99 \quad (2)$$

$$DIC = 50.1 (\pm 0.1) * SSS + 198 (\pm 5.07) + 0.9 * (year - 1989) \quad R^2 = 0.97 \quad (3)$$

To reconstruct pH and  $f\text{CO}_2$  data from SST, SSS, TA, and DIC, the PyCO2SYS package (Version 1.8.2) for Python (Humphreys et al., 2022) was employed. The dissociation constants of carbonic acid in seawater as a function of salinity and temperature defined by Millero et al. (2006) and the  $\text{KSO}_4$  dissociation constant by Dickson (1990) (Bonou et al., 2016; Monteiro et al., 2022), were utilized. The pH scale used in this study is the total scale (Marion et al., 2011). The total probable errors were estimated by propagation, leading to estimated errors of 0.041 and  $45.00 \mu\text{atm}$ , for pH and  $f\text{CO}_2$ , respectively (Millero et al., 2006). While this study exclusively presented results for TA, DIC,  $f\text{CO}_2$ , and pH, the calculated surface ocean  $\text{CO}_2$  molar fraction ( $x\text{CO}_2$ ) and partial pressure ( $p\text{CO}_2$ ) values were also.

Since the empirical models used in this paper use only SSS and time to calculate TA and DIC trends along time, these parameters, in addition to pH and  $f\text{CO}_2$ , which were calculated from the before mentioned parameters, follow the same distribution over the years of SSS data. Furthermore, the Anderson-Darling test results showed that all variables involved in this study (SSS, SST, TA, DIC, pH and  $f\text{CO}_2$ ) had non-normal distribution (Table 1) (Miot, 2017), although the mean and median values were close to each other.

TA and DIC data were normalized to mean SSS (35.4) according to the following the method described by Friis et al. (2003) (Equation 4).

$$nX_i = \frac{X_i - X^{S=0}}{S_i} * S^{ref} + X^{S=0} \quad (4)$$

Where:

$nX_i$  = normalized variable at given "i" moment

$X_i$  = variable at given "i" moment (TA or DIC)

TABLE 1 p-value of the Anderson-Darling test and measures of central tendency of the data (mean  $\pm$  standard deviation) and median (minimum and maximum values) for sea surface salinity, temperature, total alkalinity, dissolved inorganic carbon, pH and  $f\text{CO}_2$ .

Variable [unity]	p-value	Mean $\pm$ SD	Median (Min - Max)	N
Salinity	$<2.2 \cdot 10^{-16}$	$35.42 \pm 0.78$	35.62 (31.17 - 36.44)	3789
Temperature [°C]	$<2.2 \cdot 10^{-16}$	$27.71 \pm 0.94$	27.68 (24.89 - 30.01)	5669
TA [ $\mu\text{mol kg}^{-1}$ ]	$<2.2 \cdot 10^{-16}$	$2323.04 \pm 45.56$	2334.58 (2076.15 - 2382.05)	3789
DIC [ $\mu\text{mol kg}^{-1}$ ]	$<2.2 \cdot 10^{-16}$	$1988.08 \pm 39.64$	1997.70 (1777.77 - 2043.18)	3789
pH	$<2.2 \cdot 10^{-16}$	$8.0595 \pm 0.0128$	8.0591 (8.0236 - 8.0959)	3789
$f\text{CO}_2$ [ $\mu\text{atm}$ ]	$8.06 \cdot 10^{-12}$	$383.14 \pm 12.88$	382.86 (347.19 - 422.98)	3789

P-values smaller than 0.05 indicate non-normal distribution of data and "N" indicates the amount of data points for each variable.

$X^{S=0}$  = variable at 0 salinity

$S_i$  = salinity at given "i" moment

$S^{ref}$  = salinity at reference level. At this study we used the mean salinity of our data (35.42)

## 2.3 Databases for comparison

For this study, data up to 20 m depth of TA, DIC and pH measurements between latitudes  $3^\circ$  and  $10^\circ$  N and longitudes of  $28^\circ$  and  $42^\circ$  W from the GLODAPv2.2022 data product (Global Data Analysis Project) (Lauvset et al., 2022) were used, with a total of 69 TA data, 58 DIC data and 69 pH data (Figure 1). Data corresponds to the period from 1998 to 2018 and a mean depth of 9 m. GLODAP data is publicly available at <https://www.glodap.info/>. The 20 m depth was estimated based on the estimation of the regional mixed layer depth from De Boyer Montégut et al. (2004). Changes in pressure in the chosen depth do not affect TA data due to its conservative properties (Middelburg et al., 2020).

To compare with the  $f\text{CO}_2$  data calculated in this study,  $f\text{CO}_2$  data from the SOCAT platform were used (Bakker et al., 2016). The same area as used for GLODAP was selected and only data from 1998 to 2018 were accepted (totalizing 41212 data). The study also utilized daily averages of hourly  $f\text{CO}_2$  data from the CARIOCA sensor, installed in the same buoy as a reference (Lefèvre et al., 2008; Merlivat et al., 2015) from 2008 to 2011 to compare with the study's results and visualize the model's variation around actual values. Daily averages for  $f\text{CO}_2$  were preferred due to the use of daily averages of hourly SSS and SST data from the PIRATA buoy in the study. This approach aimed to prevent high-frequency variations in fugacity, observed in the region (Bruto et al., 2017), from affecting the comparison. *In situ*  $\text{CO}_2$ -related measurements obtained at  $8^\circ\text{N}$   $38^\circ$  W are already included in these global data products. GLODAP and SOCAT data description for these comparisons can be seen in Table 2.

TABLE 2 Metadata for GLODAP and SOCAT data used in this study.

Cruise	Start Time	End Time	Latitude Range	Longitude Range	Ship	Reference
06MT20021015	21/10/2002	25/10/2002	9.9 - 10	318 - 330.9	Meteor	10.3334/CDIAC/otg.MET55
06ZG20091213	16/12/2009	17/12/2009	3 - 9.0	329.9 - 332	Rio Blanco	10.3334/ CDIAC/OTG.VOS_Monte_Rio_Lines_2010
06ZG20100115	21/01/2010	22/01/2010	3 - 6.9	330.4 - 332	Rio Blanco	10.3334/ CDIAC/OTG.VOS_Monte_Rio_Lines_2010
06ZG20100207	11/02/2010	11/02/2010	3 - 9.5	329.8 - 332	Rio Blanco	10.3334/ CDIAC/OTG.VOS_Monte_Rio_Lines_2010
06ZG20100226	04/03/2010	05/03/2010	3 - 8.8	329.9 - 331.9	Rio Blanco	10.3334/ CDIAC/OTG.VOS_Monte_Rio_Lines_2010
06ZG20100321	24/03/2010	25/03/2010	3.1 - 10	329.5 - 332	Rio Blanco	10.3334/ CDIAC/OTG.VOS_Monte_Rio_Lines_2010
06ZG20100506	11/05/2010	11/05/2010	3 - 6.9	329.7 - 331	Rio Blanco	10.3334/ CDIAC/OTG.VOS_Monte_Rio_Lines_2010
06ZG20100716	23/07/2010	24/07/2010	3 - 9.8	329.7 - 332	Rio Blanco	10.3334/ CDIAC/OTG.VOS_Monte_Rio_Lines_2010
06ZG20100813	16/08/2010	17/08/2010	3 - 5.2	330.9 - 332	Rio Blanco	10.3334/ CDIAC/OTG.VOS_Monte_Rio_Lines_2010
06ZG20100902	10/09/2010	11/09/2010	4.8 - 8.9	330.5 - 332	Rio Blanco	10.3334/ CDIAC/OTG.VOS_Monte_Rio_Lines_2010
06ZG20100930	06/10/2010	06/10/2010	3.0 - 10.0	326.2 - 331.6	Rio Blanco	10.3334/ CDIAC/OTG.VOS_Monte_Rio_Lines_2010
06ZG20101023	29/10/2010	29/10/2010	3 - 6.8	330.4 - 332	Rio Blanco	10.3334/ CDIAC/OTG.VOS_Monte_Rio_Lines_2010
06ZG20101118	22/11/2010	23/11/2010	3 - 5.6	324.8 - 326.2	Rio Blanco	10.3334/ CDIAC/OTG.VOS_Monte_Rio_Lines_2010
14AT20090320	22/03/2009	31/03/2009	3.0 - 10.0	321.7 - 322.8	Antares	10.3334/ CDIAC/OTG.TSM_PIRATA_8N_38W_CRUISE
14AT20100725	25/07/2010	04/08/2010	3.0 - 10.0	321.9 - 322.1	Antares	10.3334/ CDIAC/OTG.TSM_PIRATA_8N_38W_CRUISE
29HE20001028	04/11/2000	06/11/2000	3.0 - 10.0	331.7 - 331.7	Hesperides	10.1594/PANGAEA.850338
29HE20010306	30/03/2001	01/04/2001	3.0 - 10.0	332 - 332	Hesperides	10.1594/PANGAEA.850339
29HE20011027	05/11/2001	06/11/2001	3.0 - 10.0	332 - 332	Hesperides	10.1594/PANGAEA.850340
29HE20021028	04/11/2002	06/11/2002	3 - 9.9	332 - 332	Hesperides	10.1594/PANGAEA.850342
29HE20041021	31/10/2004	02/11/2004	3.0 - 10.0	332 - 332	Hesperides	10.1594/PANGAEA.850344
29HE20051019	30/10/2005	31/10/2005	3 - 9.9	332 - 332	Hesperides	10.1594/PANGAEA.850345
29HE20060925	05/10/2006	06/10/2006	3 - 7.3	332 - 332	Hesperides	10.1594/PANGAEA.850347
29HE20070321	20/04/2007	22/04/2007	3 - 8.5	328.3 - 330.4	Hesperides	10.1594/PANGAEA.850348
33RO19990115	24/01/1999	26/01/1999	4.4 - 10	324.4 - 332	Ronald H. Brown	10.3334/CDIAC/otg.VOS_RB_1999
33RO20020201	13/02/2002	18/02/2002	3.0 - 7.0	318 - 325	Ronald H. Brown	10.3334/CDIAC/otg.VOS_RB_2002
33RO20030715	29/07/2003	30/07/2003	10-Sep	331.5 - 332	Ronald H. Brown	10.3334/CDIAC/otg.VOS_RB_2003
33RO20040301	05/03/2004	07/03/2004	6.2 - 10	318 - 327.3	Ronald H. Brown	10.3334/CDIAC/otg.VOS_RB_2004

(Continued)

TABLE 2 Continued

Cruise	Start Time	End Time	Latitude Range	Longitude Range	Ship	Reference
33RO20070505	08/05/2007	09/05/2007	7.2 - 10	325.1 - 332	Ronald H. Brown	10.3334/CDIAC/otg.VOS_RB_2007
33RO20080429	08/05/2008	10/05/2008	3.0 - 10.0	321 - 326.5	Ronald H. Brown	10.3334/CDIAC/otg.VOS_RB_2008
33RO20090711	15/07/2009	18/07/2009	3.2 - 6.7	318 - 328.1	Ronald H. Brown	10.3334/CDIAC/otg.VOS_RB_2009
33RO20130108	04/02/2013	07/02/2013	4.3 - 7	318 - 332	Ronald H. Brown	10.7289/V5P26WCZ
33RO20130901	21/09/2013	21/09/2013	9.0 - 10.0	331.5 - 332	Ronald H. Brown	10.3334/cdiac/otg.vos_rb_2013
58US20181201	16/12/2018	18/12/2018	3.0 - 10.0	331.3 - 331.4	Kronprins Haakon	10.25921/t4c7-cv15
65DK20141115	15/11/2014	15/11/2014	3 - 4.8	329.7 - 330.3	Cap San Lorenzo	10.3334/CDIAC/OTG.VOS_Cap_San_Lorenzo_2014
65DK20150228	06/03/2015	07/03/2015	3.0 - 10	329.4 - 331.9	Cap San Lorenzo	10.3334/CDIAC/OTG.VOS_Cap_San_Lorenzo_2015
65DK20150428	02/05/2015	03/05/2015	3.1 - 10	329.5 - 331.9	Cap San Lorenzo	10.3334/CDIAC/OTG.VOS_Cap_San_Lorenzo_2015
65DK20150619	26/06/2015	27/06/2015	3.0 - 10	329.5 - 332	Cap San Lorenzo	10.3334/CDIAC/OTG.VOS_Cap_San_Lorenzo_2015
65DK20150814	21/08/2015	22/08/2015	3.0 - 10	329.5 - 332	Cap San Lorenzo	10.1594/PANGAEA.878479
65DK20151009	16/10/2015	17/10/2015	3 - 8.9	329.9 - 332	Cap San Lorenzo	10.1594/PANGAEA.878481
65DK20160129	05/02/2016	06/02/2016	4.9 - 8.9	330.6 - 332	Cap San Lorenzo	10.1594/PANGAEA.878484
65DK20170104	09/01/2017	10/01/2017	3.0 - 10	329.6 - 332	Cap San Lorenzo	10.7289/V52Z13V6
65DK20170225	03/03/2017	04/03/2017	3.0 - 7.4	330.3 - 332	Cap San Lorenzo	10.7289/V52Z13V6
65DK20170423	29/04/2017	30/04/2017	3 - 7.5	330.3 - 332	Cap San Lorenzo	10.7289/V52Z13V6
65DK20170617	24/06/2017	24/06/2017	3 - 7.4	330.3 - 332	Cap San Lorenzo	10.7289/V52Z13V6
65DK20180624	02/07/2018	02/07/2018	3 - 6.1	330.6 - 332	Cap San Lorenzo	10.25921/q9p5-m569
740H20121011	28/10/2012	29/10/2012	6.5 - 10	329.3 - 331.8	James Cook	10.3334/cdiac/otg.vos_james_cook_amt22
74E320111003	17/10/2011	19/10/2011	4.8 - 10	328.6 - 332	Discovery	10.7289/V5PZ5733
74JC20131009	20/10/2013	21/10/2013	3.0 - 10	330.4 - 330.6	James Clark Ross	10.3334/cdiac/otg.vos_jcr_2013
PASR20140117	24/01/2014	25/01/2014	3 - 9.5	329.8 - 331.9	Santa Cruz	10.3334/CDIAC/OTG.VOS_Santa_Cruz_2014
06BE20001128	05/12/2000	12/12/2000	3.5 - 10	319.1 - 327.4	Sonne	10.3334/cdiac/otg.carina_06be20001128
06BE20030525	30/05/2003	02/06/2003	3 - 7.5	323.2 - 325.7	Sonne	10.3334/cdiac/otg.clivar_ar04_06be20030525
06M320150501	08/05/2015	18/05/2015	6.0 - 10	319.2 - 332	Meteor	10.7289/v5qc01tk
06MT19940219	10/03/1994	14/03/1994	3 - 4.5	318.9 - 325	Meteor	10.3334/cdiac/otg.carina_06mt19940219
06MT20020607	12/06/2002	16/06/2002	3 - 7.4	320 - 325.7	Meteor	10.3334/cdiac/otg.carina_06mt20020607

(Continued)

TABLE 2 Continued

Cruise	Start Time	End Time	Latitude Range	Longitude Range	Ship	Reference
06MT20021013	21/10/2002	25/10/2002	10.0 - 10	318.3 - 329.7	Meteor	10.3334/cdiac/otg.carina_06mt20021013
06MT20060606	10/06/2006	11/06/2006	3.0 - 5	325 - 325	Meteor	10.3334/cdiac/otg.met_68_2_2006
06MT20091126	12/12/2009	17/12/2009	6 - 9.7	329 - 332	Meteor	10.25921/0haq-t221
06MT20101014	31/10/2010	02/11/2010	7.0 - 10	332 - 332	Meteor	10.25921/wamc-d787
29HE20010305	30/03/2001	31/03/2001	4.1 - 7.1	332 - 332	Hesperides	10.3334/cdiac/otg.clivar_ficaram_ii
29HE20100405	28/04/2010	06/05/2010	7.5 - 7.5	318.5 - 331.7	Hesperides	10.3334/cdiac/otg.clivar_a06_2010
29HE20130320	30/04/2013	02/05/2013	3.5 - 9	330.7 - 331.4	Hesperides	10.3334/cdiac/otg.clivar_ficaram_xv
3.23E+11	08/03/1994	10/03/1994	3.0 - 6	318 - 323	Maurice Ewing	10.3334/cdiac/otg.ndp084
316N19821201	03/01/1983	08/02/1983	3 - 8.9	318.1 - 332	Knorr	10.3334/cdiac/otg.ttotas
32OC19880723	19/08/1988	19/08/1988	8.9 - 9.6	331.6 - 331.9	Oceanus	10.3334/cdiac/otg.woce_a16n_1988
33LK19960415	22/04/1996	12/05/1996	3 - 8.4	318.1 - 325	Edwin Link	10.3334/cdiac/otg.carina_33lk19960415
33RO20030604	29/07/2003	30/07/2003	9.0 - 10	331.5 - 332	R.H. Brown	10.3334/cdiac/otg.ndp085
33RO20130803	21/09/2013	21/09/2013	9.5 - 10	331.5 - 331.7	Ronald H. Brown	10.3334/cdiac/otg.goship_a16n_2013
35A319930102	05/02/1993	07/02/1993	07-Mar	325 - 325	L'Atalante	10.3334/cdiac/otg.woce_a07_1993
35A319930213	19/02/1993	26/02/1993	7.4 - 7.5	318 - 331.3	L'Atalante	10.3334/cdiac/otg.woce_a06_1993
35LU19950909	15/09/1995	07/10/1995	3.7 - 8.4	318 - 325	LeNoroit	10.3334/cdiac/otg.carina_35lu19950909
35TH19990712	27/07/1999	29/07/1999	3.0 - 7	325 - 325	Thalassa	10.3334/cdiac/otg.carina_35th19990712

In order to compare the surface trend with the atmospheric trend of CO<sub>2</sub>, data from the Ragged Point station, Barbados, 13°N-59°W (<http://www.esrl.noaa.gov/gmd/ccgg/iadv/>) from NOAA/Earth System Research Laboratory (ESRL) Global Monitoring Division were used, as it is the closest location to the PIRATA 8° N 38°W buoy with measurement of atmospheric CO<sub>2</sub> (Figure 2).

## 2.4 Statistical analyses

The Anderson-Darling test was used to check for the normality of our data, as it is more efficient in large databases (Razali and Wah, 2011; Miot, 2017). All variables showed non-normal distribution. To estimate the time trend for the parameters calculated in this study, a linear regression was used, in which the slope indicates the annual variation of the parameter. On the other hand, the method described by Sutton et al. (2022) was used to remove seasonality from data. The method consists of de-seasoning the time series based on monthly climatology anomalies and then calculating the linear regression of the de-seasoned data. This method reduces variability and autocorrelation in environmental datasets (Bates et al., 2014). Although the linear regression is a parametric test, it was used in order to keep an agreement with other time series studies in the field.

To compare the calculated values of TA, DIC and pH with the *in-situ* data available in GLODAP, as well as the calculated values of

*f*CO<sub>2</sub> with the data from SOCAT, the Wilcoxon-Mann-Whitney test was used. This same test was also used to evaluate if the two seasons observed in this study were statistically different. *p*-values < 0.05 reject the null hypothesis, suggesting statistical differences in medians and population divergence.

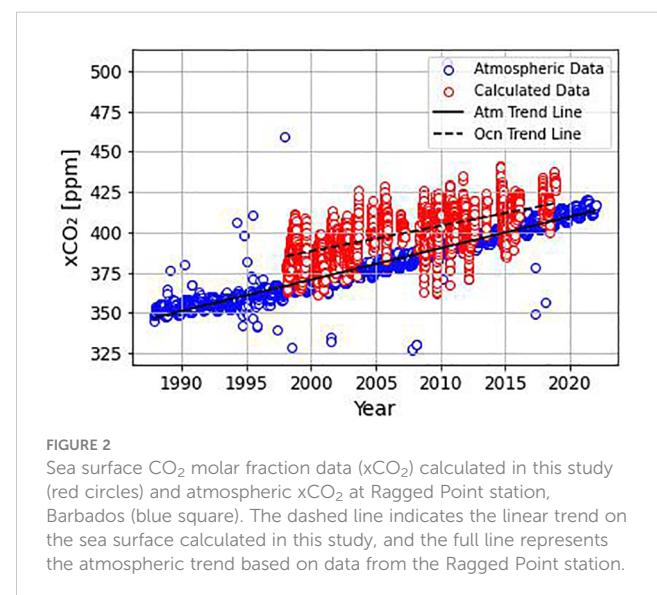


FIGURE 2  
Sea surface CO<sub>2</sub> molar fraction data (xCO<sub>2</sub>) calculated in this study (red circles) and atmospheric xCO<sub>2</sub> at Ragged Point station, Barbados (blue square). The dashed line indicates the linear trend on the sea surface calculated in this study, and the full line represents the atmospheric trend based on data from the Ragged Point station.

## 3 Results

### 3.1 Seasonality

Based on the monthly variation of rain rate, two characteristic periods were observed (Figure 3): one from July to December with high rainfall ( $0.67 \pm 0.82 \text{ mm h}^{-1}$ ), here called the wet season, and a period from January to June with lower rates of rainfall ( $0.23 \pm 0.44 \text{ mm h}^{-1}$ ), here called the dry season. Both seasons showed statistically significant difference through the Mann-Whitney test (rainfall, SSS, SST, TA, DIC, pH and  $f\text{CO}_2$  presented p-values smaller than 0.05).

Mean SST varied in a similar way as mean rainfall, with lower values during dry season ( $26.99 \pm 0.50^\circ\text{C}$ ) and higher values during wet season ( $28.34 \pm 0.43^\circ\text{C}$ ), while mean SSS varied opposite to mean rainfall, with higher values during dry season ( $35.94 \pm 0.27$ ) and lower values during wet season ( $35.01 \pm 0.58$ ). The monthly calculated mean TA and DIC followed the SSS variation, with higher values during dry season, with a mean value of  $2352.9 \pm 16.0 \mu\text{mol kg}^{-1}$  for TA and  $2013.8 \pm 15.6 \mu\text{mol kg}^{-1}$  for DIC, and lower values during wet season, with a mean value of  $2299.2 \pm 33.6 \mu\text{mol kg}^{-1}$  for TA and  $1967.4 \pm 29.2 \mu\text{mol kg}^{-1}$  for DIC. Calculated pH showed a monthly variation similar to that of salinity, with a standard deviation similar between the two seasons, but higher values during dry season, mean of  $8.066 \pm 0.011$ , and lower values during wet season, with a mean value of  $8.054 \pm 0.010$ . The observed

similarity in pH values, even when considering 2–3 decimal places, warrants discussion regarding potential differences in other variables during these periods. While our study focused on analyzing pH and temperature and salinity variations, it is essential to acknowledge the influence of additional factors such as dissolved oxygen levels, and nutrient concentrations, may have contributed to the observed patterns. Further investigation into these variables could provide insights into the underlying mechanisms driving the observed pH variations between seasons. Calculated surface ocean  $\text{CO}_2$  fugacity ( $f\text{CO}_2$ ), on the other hand, showed the opposite variation in comparison to SSS, with lower values during dry season, mean of  $380.0 \pm 11.7 \mu\text{atm}$ , and higher values during wet season, with a mean value of  $385.4 \pm 12.9 \mu\text{atm}$ .

### 3.2 Comparison with other databases

TA, pH and  $f\text{CO}_2$  had statistically significant differences (p-value < 0.05) (Table 3), with this study underestimating the values (Table 1) when compared to GLODAP (Figure 4) and SOCAT (lower medians) (Figure 5); yet DIC didn't have statistically significant differences (p-value  $\geq 0.05$ ), although it had lower median than the one from GLODAP data. However, when separating the data according to the season (dry and wet), it was possible to observe that, in the dry season, all parameters showed statistically different medians (p-value < 0.05), with the exception of

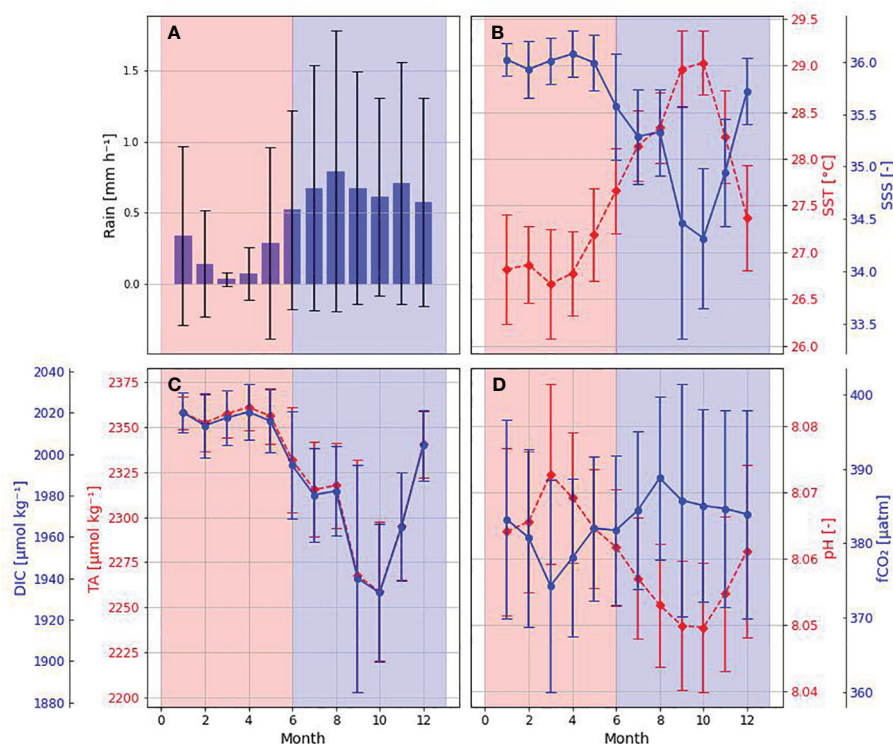


FIGURE 3

Climatology of observed and estimated parameters at the PIRATA buoy  $8^\circ\text{N}$ - $38^\circ\text{W}$  based on monthly means. (A) Rain rate ( $\text{mm h}^{-1}$ ); (B) Sea surface salinity (blue dots) and temperature ( $^\circ\text{C}$ , red dots); (C) Total alkalinity ( $\mu\text{mol kg}^{-1}$ , blue dots) and dissolved inorganic carbon ( $\mu\text{mol kg}^{-1}$ , red dots); (D) pH (red dots) and  $\text{CO}_2$  fugacity ( $f\text{CO}_2$ , in  $\mu\text{atm}$ , blue dots). The bars at each month at (A–D) indicate the standard deviation. Red shaded areas in the plots represent dry season (January to June) and blue shaded areas, wet season (July to December).

**TABLE 3** Medians (Md – calculated in this study, md – data available in GLODAP or SOCAT) and p-value of the Wilcoxon-Mann-Whitney test for surface total alkalinity (TA, in  $\mu\text{mol kg}^{-1}$ ), dissolved inorganic carbon (DIC, in  $\mu\text{mol kg}^{-1}$ ), pH and  $\text{CO}_2$  fugacity ( $f\text{CO}_2$ , in  $\mu\text{atm}$ ) using all data, dry season data (from January to June) and wet season data (from July to December).

Variable	All data	Dry season	Wet season
	md	Md-md	Md-md
	p-value	p-value	p-value
	(N/n)	(N/n)	(N/n)
TA <sup>a</sup>	2361.8	2356.8-2364.5	2305.3-2327
	5.86 10 <sup>-11</sup>	0.001	0.0002
	(3789/69)	(1914/50)	(1875/19)*
DIC <sup>a</sup>	2003.1	2016.8-2009.5	1972.6-1974.9
	0.046	0.61	0.27
	(3789/58)	(1914/38)*	(1875/20)*
pH <sup>a</sup>	8.062	8.065-8.058	8.054-8.081
	0.049	7.57 10 <sup>-6</sup>	7.58 10 <sup>-9</sup>
	(3789/69)	(1914/51)	(1875/18)
$f\text{CO}_2$ <sup>b</sup>	381.1	381.2-376.8	384.8-385.1
	2.69 10 <sup>-8</sup>	6.07 10 <sup>-15</sup>	0.74
	(3789/41212)	(1679/15650)	(1875/25562)*

"N" stands for the amount of data points calculated in this study while "n" stands for the number of data points available in GLODAP or SOCAT.

<sup>a</sup>Compared with data from GLODAPv2.2022 between 3° and 10°N and 28° 42°W (Lauvset et al., 2022).

<sup>b</sup>Compared SOCAT data version 2023 (Bakker et al., 2016).

\*Represents statistically equal medians with a confidence interval of 95%.

pH. On the other hand, during wet season, only TA showed statistically equal medians (p-value  $\geq 0.05$ ), while DIC, pH and  $f\text{CO}_2$  showed p-values smaller than 0.05.

### 3.3 Trends over time

DIC, pH, and  $f\text{CO}_2$  exhibited significant trends over time based on not de-seasoned data (Table 4). The trends included a yearly increase of  $0.7 \mu\text{mol kg}^{-1}$  for DIC, a decrease of 0.001 pH units per year for pH, and an increase of  $1.539 \mu\text{atm}$  per year for  $f\text{CO}_2$  (Figure 6). Notably, when data was de-seasoned, only pH and  $f\text{CO}_2$  retained significant trends (pH =  $-0.001 \pm 0.000 \text{ year}^{-1}$ ;  $f\text{CO}_2 = +1.633 \pm 0.108 \mu\text{atm year}^{-1}$ ) (Figure 7). Additionally, when dry and wet seasons were analyzed separately (Table 5), all variables except SST exhibited significant trends. Notably, the SSS and TA data showed opposing trends between seasons, with positive trends during the dry season and negative trends during the rainy season, emphasizing the seasonal variability. The oceanic  $x\text{CO}_2$  time series showed an increase around 17% lower than those reported for Barbados station ( $1.908 \pm 0.010 \text{ ppm year}^{-1}$ ). This delay in our trend related to the atmospheric data highlights the weaker absorption trend of atmospheric  $\text{CO}_2$  by the WTA.

### 3.4 Data normalization

The normalization of TA and DIC data (Figure 8) highlighted 3 different aspects of these carbonate parameters: (1) TA-SSS relationship did not vary significantly after normalization, (2) the increase in DIC with time became more apparent (trend of  $0.897 \pm 0.001 \mu\text{mol kg}^{-1}\text{year}^{-1}$  and, (3) the normalized pH and  $f\text{CO}_2$  trends

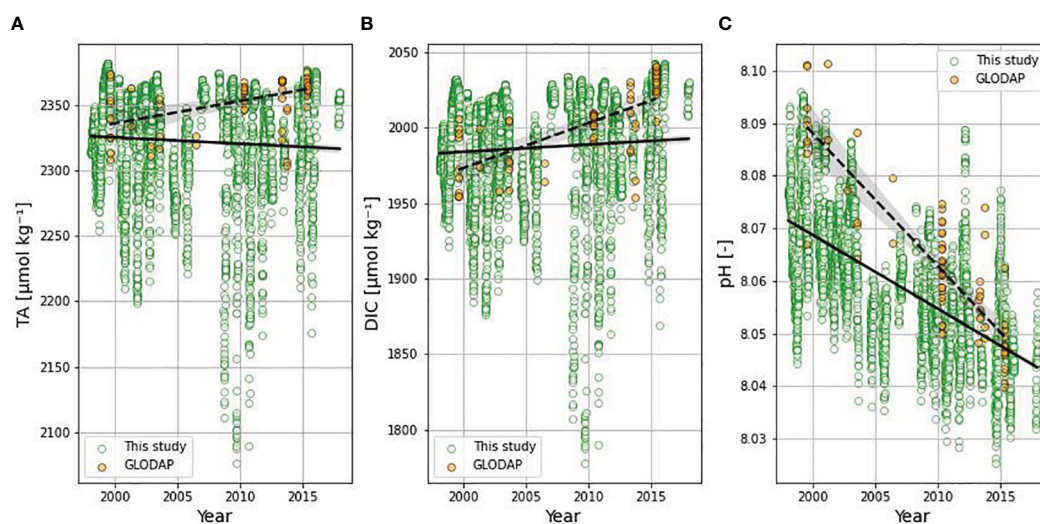


**FIGURE 4**

Time series of: (A) TA, (B) DIC, (C) pH. Green dots represent this study's data and orange dots represent GLODAP's data from 1998 to 2018, up to 20m depth and between latitudes 3° and 10° N and longitudes of 28° and 42°W. The solid line represents the trend in this study's data, while the dashed line represents the trend in GLODAP's data (Lauvset et al., 2022).

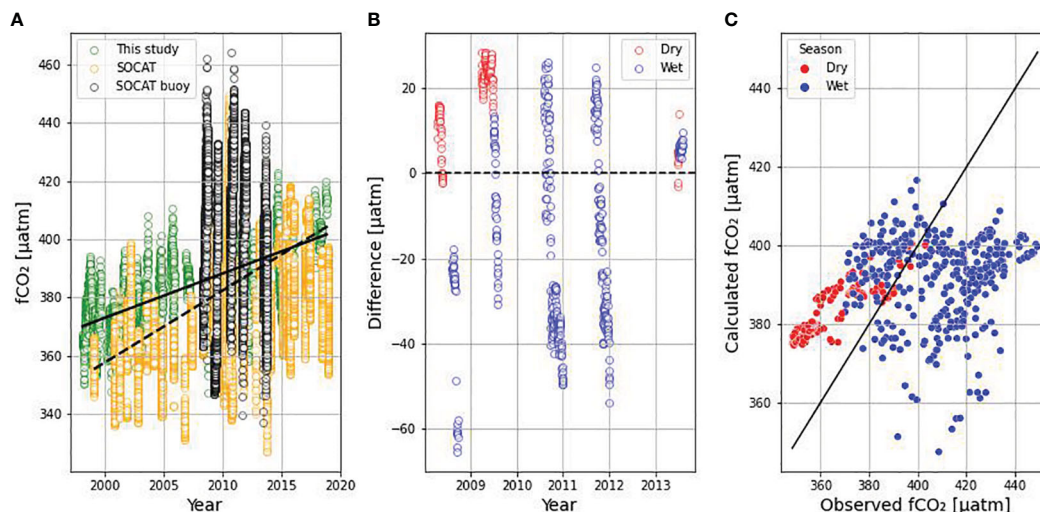


**FIGURE 5** Comparison between  $fCO_2$  data calculated in this study and observed  $fCO_2$  data from SOCAT (Bakker et al., 2016) from 1998 to 2018 and between latitudes  $3^\circ$  and  $10^\circ$  N and longitudes of  $28^\circ$  and  $42^\circ$  W. (A) Time series with this study's data (green dots), SOCAT's data (orange dots) and data from the CARIOCA sensor installed on the buoy from 2008 to 2011 (black dots); (B) Difference between this study's data and SOCAT's data (Positive values indicate overestimation and negative values indicate underestimation; red dots represent dry season and blue dots, wet season); (C) Dispersion plot between the two datasets (red and blue dots indicate dry and wet seasons, respectively, and the black line represents the 1: 1 line between the observed data and the calculated data).

subsequently calculated did not show bigger changes after normalization ( $-0.001 \pm 0.001$  and  $1.538 \pm 0.026$ , respectively).

### 4 Discussion

The study area is susceptible to large seasonal variability in surface salinity (Field, 2007; Grodsky et al., 2014) which is reflected in the parameters of the marine carbonate system (Bonou et al., 2016; Bruto et al., 2017). The wet season englobes both the months of the largest discharges of freshwater of the Amazon River and the months in which its waters reach the easternmost area in the Western Tropical Atlantic (Bonou et al., 2016). That and the addition of the rainfall associated to the ITCZ promote a decrease of local sea surface salinity, diluting TA and DIC, as well. These 3 parameters were described by Monteiro et al.

(2022) as important drivers of seasonal  $pCO_2$  variations in the Western Tropical Atlantic, with DIC and TA being the most expressive one in the NECC region. Thus, it is difficult to capture this variability using available GLODAP *in situ* data for the region (Lauvset et al., 2022). This emphasizes the importance of using empirical models in the reconstruction of parameters of the marine carbonate system, since these techniques can be used to fill the gaps left by the lack of data in oceanic regions. The lack of *in situ* data reflecting the temporal and spatial variability in the western tropical Atlantic has also been highlighted by Monteiro et al. (2022). The months from September to November in the years 2008 to 2010 recorded the lowest values of SSS, TA, and DIC (Figure 9). Foltz et al. (2012) attributed this phenomenon to an anomalous sea surface cooling in the Northern Equatorial Atlantic at the beginning of 2009, that caused an abnormal southward shift of the ITCZ over the South American continent. The observed

**TABLE 4** Data trend over time for sea surface salinity, temperature, total alkalinity (TA), dissolved inorganic carbon (DIC), pH and  $CO_2$  fugacity ( $fCO_2$ ), as well as pH and  $fCO_2$  de-seasoned data trends.

Variable [unity]	p-value	R <sup>2</sup>	N	Slope ± error [Unity year <sup>-1</sup> ]	p-value (de-seasoned)	R <sup>2</sup> (de-seasoned)	N (de-seasoned)	Slope ± error [Unity year <sup>-1</sup> ] (de-seasoned)
Salinity	0.093	0.00075	3789	$-0.0036 \pm 0.0021$				
Temperature [°C]	0.095	0.0005	5669	$0.0039 \pm 0.0023$				
TA [ $\mu\text{mol kg}^{-1}$ ]	0.093	0.00075	3789	$-0.209 \pm 0.124$				
DIC [ $\mu\text{mol kg}^{-1}$ ]	$3.1 \cdot 10^{-11} *$	0.01158	3789	$0.717 \pm 0.108$				
pH	$<2.2 \cdot 10^{-16} *$	0.418	3789	$-0.0014 \pm 0.0001$	$<2.2 \cdot 10^{-16} *$	0.725	145	$-0.0014 \pm 0.0001$
$fCO_2$ [ $\mu\text{atm}$ ]	$<2.2 \cdot 10^{-16} *$	0.489	3789	$1.515 \pm 0.025$	$<2.2 \cdot 10^{-16} *$	0.69	145	$1.633 \pm 0.091$

p-value comes from the linear regression, with \* marking statistically significant trend over time, R<sup>2</sup> is the coefficient of determination of linear regression, "N" is the amount of data for the variable, slope is the trend of the variable per year and error is the standard error regarding the slope of the line.

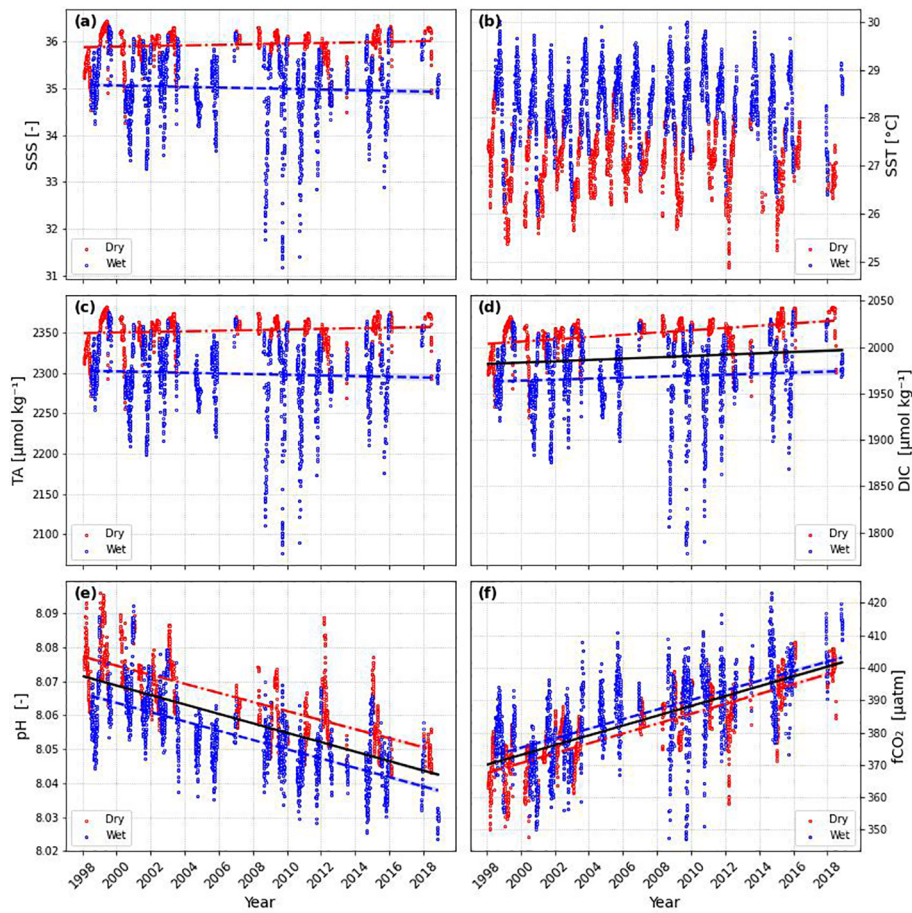


FIGURE 6

Time series of: (A) Sea Surface Salinity (SSS), (B) Sea Surface Temperature (SST), (C) Total Alkalinity (TA), (D) Dissolved Inorganic Carbon (DIC), (E) pH and (F) Carbon dioxide Fugacity ( $fCO_2$ ). Red dots represent dry season and blue dots represents the wet season. The red dot-dashed line represents the trend in the dry season, the solid black line represents the whole period trend, and the blue dashed line represents the trend in the wet season. Lines are shown only when the trend is statistically significant ( $p$ -value < 0.05).

lower salinity is likely associated with the anomalous flood of the Amazon River (Chen et al., 2010).

Based on the analysis done in this study, the calculated  $fCO_2$  data exhibited a slight upward deviation when compared to the

corresponding data from the SOCAT database (Figure 5A). However, this difference was relatively small, with a median ratio of 0.45%. Interestingly, upon excluding data from the buoy, this disparity noticeably increased to 2.88%. It is noteworthy that the

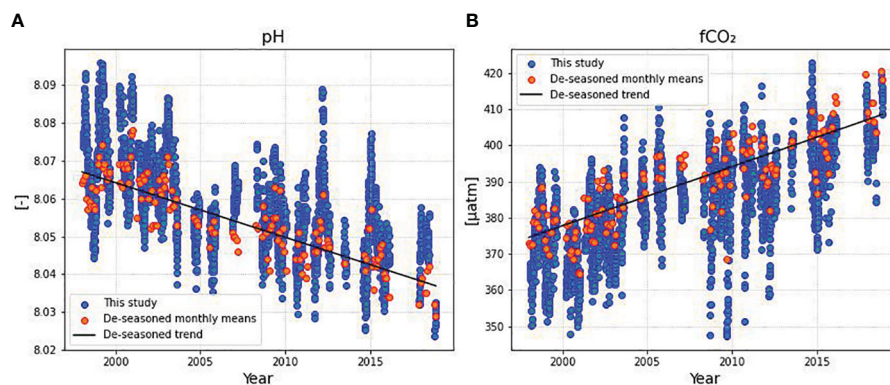


FIGURE 7

Time series of: (A) pH and (B)  $fCO_2$ . Blue dots represent the original time series and red dots represents de-seasoned monthly means. Linear trend was calculated based on de-seasoned data.

TABLE 5 Data trend separated in dry (January to June) and wet season (July to December) for sea surface salinity, temperature, total alkalinity (TA), dissolved inorganic carbon (DIC), pH and CO<sub>2</sub> fugacity (fCO<sub>2</sub>).

Variable [unity]	Season (Mean ± Standard deviation)	p-value	R <sup>2</sup>	Slope ± error [Unity year <sup>-1</sup> ]
Salinity	Dry (35.9 ± 0.3)	8.69 10 <sup>-7</sup> *	0.014	0.006 ± 0.001
	Wet (35.0 ± 0.4)	0.020 *	0.003	-0.007 ± 0.003
Temperature [°C]	Dry (26.9 ± 0.5)	0.98	1.58 10 <sup>-7</sup>	-0.0004 ± 0.00213
	Wet (28.3 ± 0.4)	0.91	4.37 10 <sup>-6</sup>	0.0003 ± 0.0024
TA [μmol kg <sup>-1</sup> ]	Dry (2352.9 ± 16.0)	8.69 10 <sup>-7</sup> *	0.014	0.377 ± 0.076
	Wet (2299.2 ± 33.6)	0.020 *	0.0025	-0.4146 ± 0.1775
DIC [μmol kg <sup>-1</sup> ]	Dry (2013.8 ± 15.6)	<<0.001*	0.1709	1.2287 ± 0.0661
	Wet (1967.4 ± 29.2)	0.0004*	0.0058	0.5378 ± 0.1530
pH	Dry (8.066 ± 0.011)	<<0.001*	0.54	-0.0013 ± 0.00003
	Wet (8.054 ± 0.010)	<<0.001*	0.47	-0.0014 ± 0.00003
fCO <sub>2</sub> [μatm]	Dry (379.99 ± 11.65)	<<0.001*	0.63	1.523 ± 0.029
	Wet (385.41 ± 12.89)	<<0.001*	0.41	1.477 ± 0.039

P-value comes from linear regression, with \* marking statistically significant trend over time, R<sup>2</sup> is the coefficient of determination of linear regression, slope is the trend of the variable per year and error is the standard error regarding the slope of the line.

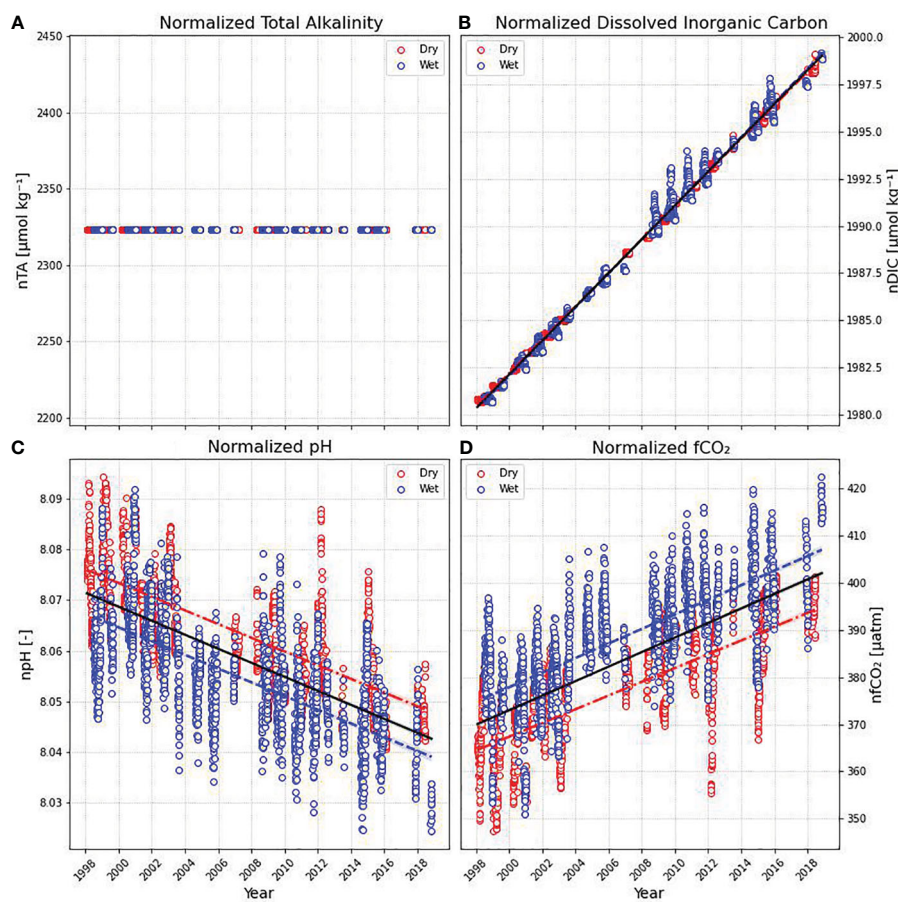


FIGURE 8 Normalized (A) total alkalinity and (B) dissolved inorganic carbon at mean sea surface salinity of 35.4. Calculated (C) pH and (D) fCO<sub>2</sub> based on normalized TA and DIC are also shown. Trend lines are shown for statistically significant trends (red: dry season, blue: wet season and black: all data).

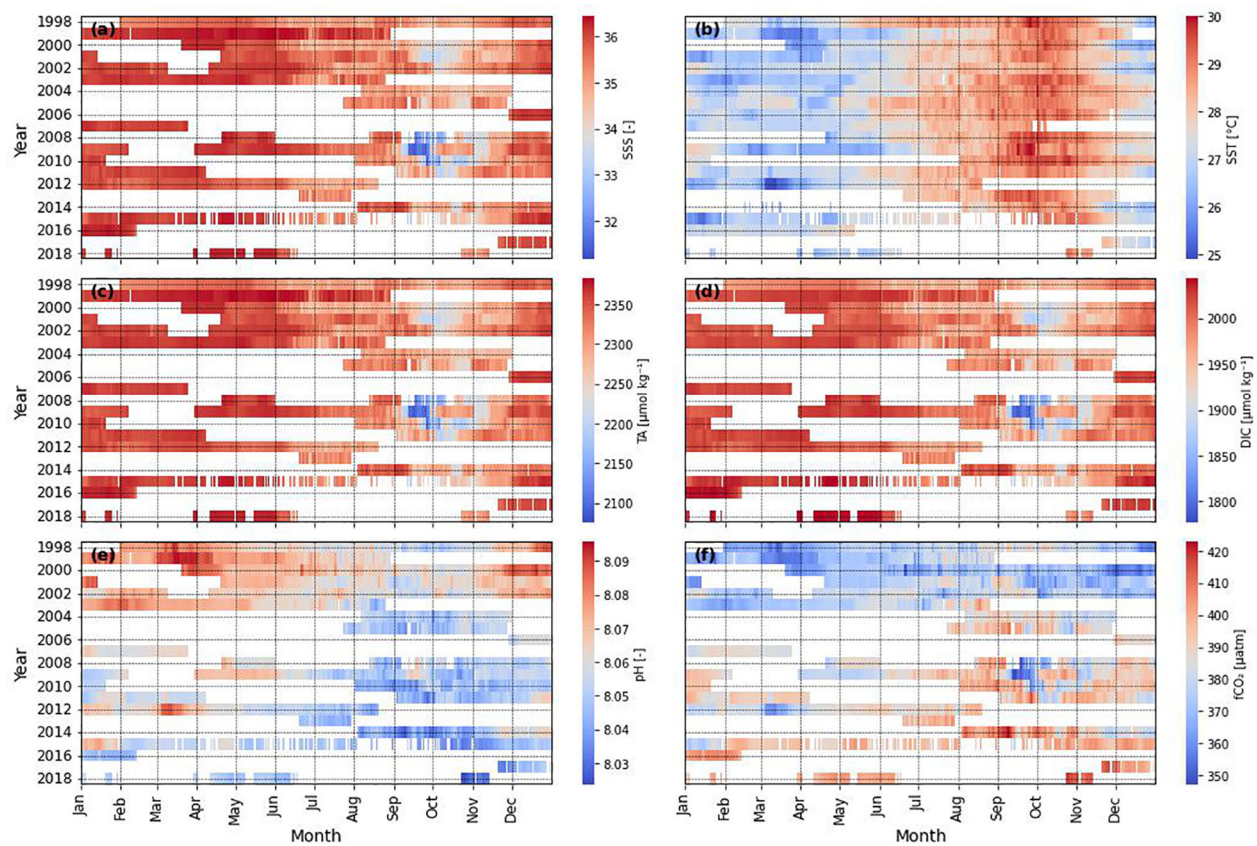


FIGURE 9  
Heatmaps of (A) SSS, (B) SST, (C) TA, (D) DIC, (E) pH and (F)  $f\text{CO}_2$ . Each cell represents a daily value.

buoy dataset, characterized by a higher frequency and greater variability, played a significant role in mitigating the observed deviation. During the period with buoy data, though, SOCAT data exhibited a higher amplitude that our calculations did not fully capture. Daily averages of the data measured by the sensor installed in the buoy showed that our calculations mostly overestimated the  $f\text{CO}_2$  values, particularly during the dry season (Figure 5B), where an overestimation of 3.11% was found when comparing the medians. This might be a result of the models used to calculate the TA and DIC that are based on the whole Western Tropical Atlantic area, which includes areas with higher salinity and lower influences of the Amazon River plume and ITCZ (Araujo et al., 2019; Bonou et al., 2022). The difference is more variable during the wet season, but still our calculations tend to underestimate the  $f\text{CO}_2$  in the area by roughly 5.51%. Considering the biological impacts in ocean carbonate parameters in the models used in this study might also affect the calculations, especially in the wet season, a time when the high nutrient plume reaches eastern parts of the Tropical Atlantic. The enhancement of primary production in the Western Tropical Atlantic by the nutrient rich Amazon River Plume is estimated to increase the oceanic's capacity of absorbing atmospheric  $\text{CO}_2$  from 30% to even 100 times (Ternon et al., 2000; Cooley et al., 2007). It is possible to see that there is no 1:1 ratio (Figure 5C) between the data calculated in this study and the data from the sensor. However, when

comparing with the graph made by Bonou et al. (2016) it is observed that, for data from the NECC region, the distribution of points of the data used in this study is similar to the point cloud showed by the aforementioned authors. This variation may be a result of primary productivity being enhanced at the region once the Amazon River plume brings waters richer in nutrients when compared to the surrounding ocean (Lefèvre et al., 2017).

The SSS, SST and  $f\text{CO}_2$  values in dry and wet seasons are in accordance to those found by Lefèvre et al. (2014) in March 2009 and July 2010 during the PIRATA XI and XII commissions, respectively. In March 2009 (July 2010), they observed an average SSS of  $35.89 \pm 0.17$  ( $35.75 \pm 0.6$ ), an average SST of  $26.3 \pm 0.8^\circ\text{C}$  ( $28.67 \pm 0.72^\circ\text{C}$ ) and average  $f\text{CO}_2$  of  $374.3 \pm 13$   $\mu\text{atm}$  ( $381.2 \pm 11.8$   $\mu\text{atm}$ ). The authors discuss the possible drivers of  $f\text{CO}_2$  variability in the region, bringing the influence of the ITCZ as an important factor in that regard. The highest values of  $f\text{CO}_2$  happening during wet season coincides with the upwelling period observed by Bruto et al. (2017) in the same study region. The authors calculated Ekman pumping from monthly wind averages with a spatial scale of  $0.25^\circ$  and identified that upwelling is more intense in the second half of the year, injecting  $\text{CO}_2$ -rich subsurface waters into the surface.

Bonou et al. (2016) found similar values to those presented in this study for SSS, SST, TA and DIC, also separating into two seasons. The average values of the dry season ( $\text{SSS} = 35.4 \pm 0.7$ ,

SST =  $27.6 \pm 1.1^\circ\text{C}$ , TA =  $2331 \pm 54 \mu\text{mol kg}^{-1}$ , DIC =  $1978 \pm 45 \mu\text{mol kg}^{-1}$ , and of the wet season (SSS =  $35.2 \pm 0.8$ , SST =  $28.1 \pm 0.8^\circ\text{C}$ , TA =  $2328 \pm 48 \mu\text{mol kg}^{-1}$ , DIC =  $1970 \pm 42 \mu\text{mol kg}^{-1}$ ) also show accuracy of these models in estimating the TA and DIC in the region. The models also showed values close to the GLODAP TA, DIC and pH data (Figure 4), with the database values in the range of the calculated parameters. When compared to the results of Bonou et al. (2022) in the Western Atlantic, we can see the mean values of TA and DIC values calculated here are higher than the ones found by them. These differences show once more the heterogeneity of the region, especially when the Amazon River Plume region (western to  $43^\circ\text{W}$ ) is added to the equation.

The combination of the intense rainfall (Figure 3A) and the Amazon River plume (Richey et al., 1989; Silva et al., 2010; Marengo and Espinoza, 2016), leads to lower surface salinity during the wet season. This, along with heating and reduced vertical mixing due to surface water stratification from added fresh water, explains higher temperatures in stronger upwelling seasons. This can also lead to the formation of more severe storms and hurricanes of higher categories (Ffield, 2007; Grodsky et al., 2012). The upwelling of subsurface water generated by tropical storm winds plays an important role in high frequency variations (less than one day) in  $f\text{CO}_2$ , thus affecting the  $\text{CO}_2$  flux in the region (Mahadevan et al., 2011; Bruto et al., 2017).

Studies investigating the trend in carbonate parameters in the Atlantic Ocean show the heterogeneity of the area and how the Western Tropical Atlantic might fit in the dynamics of the region. Lauvset et al. (2015) observed for the Equatorial Atlantic biome (between  $5^\circ\text{S}$  and  $5^\circ\text{N}$ ) a pH trend of  $-0.0016 \pm 0.0003 \text{ units year}^{-1}$  and  $f\text{CO}_2$  trend of  $1.81 \pm 0.32 \mu\text{atm year}^{-1}$ , which is in accordance to the trends observed in this study.

Further north, in the Cariaco basin, Venezuela, the CARIACO time series (CARbon Retention In A Colored Ocean,  $10.5^\circ\text{N}$ - $64.67^\circ\text{W}$ ) was conducted, with TA and pH measurements taken from 1995 to 2015 (Table 6). Bates et al. (2014) observed a significant trend in pH ( $-0.0025 \pm 0.0004 \text{ year}^{-1}$ ) which was greater than the trend observed in this study. Due to its location further west in the Caribbean Sea compared to the PIRATA buoy at

$8^\circ\text{N}$ , other factors such as regional circulation or its position over a trench may influence the local carbonate system differently than in oceanic areas (Astor et al., 2017, 2013, 2005; Muller-Karger et al., 2001).

At the BATS time series station (Bermuda Atlantic Time-series Study,  $32^\circ\text{N}$ ,  $64^\circ\text{W}$ ), in operation since 1983, Bates and Johnson (2020) calculated the time trends of marine carbonate system parameters up to 2020. The DIC time trend values ( $1.26 \pm 0.04 \mu\text{mol kg}^{-1} \text{ year}^{-1}$ ), pH ( $-0.0019 \pm 0.0001 \text{ pH units year}^{-1}$ ), and  $f\text{CO}_2$  ( $1.92 \pm 0.08 \mu\text{atm year}^{-1}$ ) were higher in magnitude than those found in this study. Unlike the BATS station, the western Tropical Atlantic does not exhibit the trend of seawater salinization, but rather shows a desalinization trend during the wet season. This indicates a possible intensification of the hydrological cycle, which could impact the  $\text{CO}_2$  dynamics in the area in the future (Byrne et al., 2018).

At the Eastern Tropical Atlantic Ocean, the European Station for Time series in the Ocean at the Canary Islands (ESTOC,  $29.04^\circ\text{N}$ - $15.5^\circ\text{W}$ ), maintains a monitoring base similar to BATS, where measurements started in 1995. Santana-Casiano et al. (2007) observed an increasing trend in the DIC ( $0.41 \pm 0.12 \mu\text{mol kg}^{-1} \text{ year}^{-1}$ ) smaller than the one found in this study, a trend towards a reduction in pH ( $-0.0017 \pm 0.0004 \text{ pH units year}^{-1}$ ) and tendency of increase in  $f\text{CO}_2$  ( $1.55 \pm 0.43 \mu\text{atm year}^{-1}$ ) close to those observed in this study. Although this station is in the eastern Atlantic Ocean, a region with a very marked and almost permanent upwelling, its annual trends are closer to the trends found in this study than those found in BATS, which is also on the western edge.

According to Monteiro et al. (2022), SSS only acts as the main driver in  $p\text{CO}_2$  variations in the Amazon River Plume region (being responsible for the biggest variation in the regional values), with the SST being the main driver of  $p\text{CO}_2$  variations in NECC region. This is contradicted by our results, since after calculating the thermal to non-thermal effects ratio on  $f\text{CO}_2$  described by Takahashi et al. (2002) we arrived at a value of 0.82, indicating that biological effects override thermal effects in  $\text{CO}_2$  variations in our area. It is important to note that the high SSS variation closer to the river might impact the results of the calculations (Jiang et al., 2014). In addition, Monteiro et al. (2022) found a trend around  $2.27 \pm 0.21$

TABLE 6 Trends in the surface carbonate system in the western Tropical Atlantic Ocean used for comparison in this study.

Region	Period	DIC [ $\mu\text{mol kg}^{-1} \text{ year}^{-1}$ ]	pH [ $\text{year}^{-1}$ ]	$f\text{CO}_2$ [ $\mu\text{atm year}^{-1}$ ]	Author
Cariaco Bay, Venezuela ( $10.5^\circ\text{N}$ - $64.67^\circ\text{W}$ )	1995 - 2015	-	$-0.0025 \pm 0.0004$	-	Bates et al. (2014)
BATS ( $32^\circ\text{N}$ - $64^\circ\text{W}$ )	1983 - 2020	$1.26 \pm 0.08$	$-0.0019 \pm 0.0001$	$1.92 \pm 0.08$	Bates and Johnson (2020)
ESTOC ( $24.04^\circ\text{N}$ - $15.5^\circ\text{W}$ )	1995 - 2004	$0.41 \pm 0.12$	$-0.0017 \pm 0.0004$	$1.55 \pm 0.43$	Santana-Casiano et al. (2007)
Equatorial Atlantic ( $5^\circ\text{S}$ - $5^\circ\text{N}$ in the Atlantic Ocean)	1991 - 2011	-	$-0.0016 \pm 0.0030$	$1.81 \pm 0.32$	Lauvset et al. (2015)
WTA at the NBC - NECC sector	1993 - 2019	$1.22 \pm 0.30$	-	$2.27 \pm 0.21^*$	Monteiro et al. (2022)
WTA ( $8^\circ\text{N}$ - $38^\circ\text{W}$ )	1998 - 2018	$0.72 \pm 0.11$	$-0.0014 \pm 0.0001$	$1.54 \pm 0.03$	this study (2023)

\*- Monteiro et al. (2022) reported their estimates in  $p\text{CO}_2$  ( $\mu\text{atm}$ ).

$\mu\text{atm year}^{-1}$ , roughly 50% higher than the trend we found in this study. However, the temperature normalized  $p\text{CO}_2$  presented a trend in time closer to the one observed in this study ( $1.56 \pm 0.26 \mu\text{atm year}^{-1}$ ), indicating that the  $p\text{CO}_2$  estimations in the NECC using the models utilized in this study tend to leave out the impact of changes in temperature (Takahashi et al., 2002).

The SST did not show a significant trend in this study, unlike neighboring regions such as the central tropical Atlantic and the Sargasso Sea, in the subtropical Atlantic, which showed an increase of  $0.009$  and  $0.021^\circ\text{C year}^{-1}$ , respectively (Deser et al., 2010; Bates and Johnson, 2020). In agreement with the data showed in this study, Friedman et al. (2017) observed that the area in this study showed no statistically significant SSS trend from 1896 to 2013 (118 years), although some studies indicate that there is a tendency towards salinization in the tropical and subtropical Atlantic Ocean (Boyer, 2005; Bates and Johnson, 2020). SSS showed, nonetheless, a trend in time only after separating data in two seasons, which might indicate a change in the hydrological cycle in the area, possibly leading to changes in the  $\text{CO}_2$  solubility in the region (Ashton et al., 2016).

In oceanic areas, trends in pH and  $f\text{CO}_2$  mainly respond to DIC fluxes on the surface, reflecting the increase in the concentration of

atmospheric  $\text{CO}_2$  (Lauvset et al., 2015). In the NECC region, in addition to DIC, temperature is an important driver in  $f\text{CO}_2$  (Monteiro et al., 2022), since the physical pump is the main driver of  $\text{CO}_2$  drawdown. Taking that in account, the lack of a temperature factor in the models for TA and DIC in the NECC area might underestimate the results for a region with less impact from the Amazon River Plume but still susceptible to high salinity seasonality.

The DIC/TA ratio is a key indicator of the acid-base equilibrium in seawater (Cai et al., 2020). A trend of  $0.0004 \pm 5.7 \cdot 10^{-7} \text{ year}^{-1}$  is observed in the study area (Figure 10A), indicating a decrease in its buffer capacity. In addition, the difference between total alkalinity and dissolved inorganic carbon (TA-DIC) is also a good tool to imply the ocean acidification (Figure 10B), with the advantage of being a conservative quantity, particularly useful in studies involving the mixing of different water masses. In this study, the TA-DIC showed a decrease of  $0.93 \pm 0.02 \mu\text{mol kg}^{-1} \text{ year}^{-1}$ , reinforcing again the decrease in buffer capacity of the region. Xue and Cai (2020) estimated a decrease in TA-DIC of around  $0.82 \mu\text{mol kg}^{-1} \text{ year}^{-1}$  at Hawaii Ocean Time-series (HOT) station. Their results suggest that the Western Tropical Atlantic is absorbing atmospheric  $\text{CO}_2$  at a more pronounced rate.

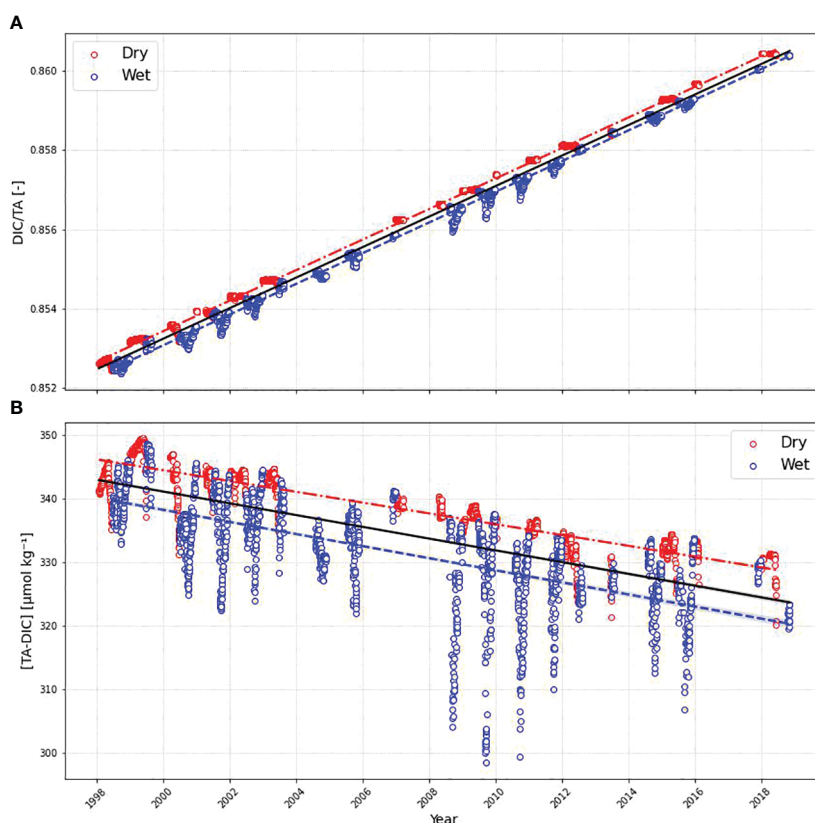


FIGURE 10

Time series of: (A) DIC/TA and (B) [TA-DIC]. Red dots represent dry season and blue dots represents the wet season. The red dot-dashed line represents the trend in the dry season, the solid black line represents the whole period trend, and the blue dashed line represents the trend in the wet season. Lines are shown only when the trend is statistically significant ( $p\text{-value} < 0.05$ ).

## 5 Conclusion

Showcasing a temporal overview of the marine carbonate system at 8°N 38°W between 1998 and 2018, our study focuses on a region distinguished by pronounced salinity variations compared to other tropical oceanic areas. This study highlights the seasonality of Total Alkalinity (TA), Dissolved Inorganic Carbon (DIC), pH, and  $f\text{CO}_2$  in the Western Tropical Atlantic (WTA), a phenomenon previously observed only on a limited time scale (Bruto et al., 2017) or across extensive spatial dimensions with intermittent temporal continuity (Körtzinger, 2003; Lefèvre et al., 2010; Bonou et al., 2016). In this study, no significant SSS trend was observed from 1998 to 2018, agreeing with the trend calculated from data collected *in situ* in the Atlantic in the same region from 1896 to 2013 (Friedman et al., 2017), although a positive and negative trend can be observed in dry and wet seasons, respectively. This could possibly lead to the increase of high frequency variability in  $f\text{CO}_2$  due to upwelling by tropical storm winds (Ffield, 2007; Mahadevan et al., 2011; Grodsky et al., 2012). SST also showed no significant trend, diverging from studies showing an increase in SST both in the Central Tropical Atlantic and in the BATS time series (Deser et al., 2010; Bates and Johnson, 2020).

From the comparison with other studies analyzing the trend of parameters in the marine carbonate system in the tropical and subtropical Atlantic, it was observed that the increase in DIC and  $f\text{CO}_2$ , in addition to the reduction in pH, were smaller when compared to the observed trends in CARIACO and BATS (Bates et al., 2014; Bates and Johnson, 2020). On the other hand, the ESTOC station, on the eastern edge of the Tropical Atlantic, showed a smaller increase in DIC, a stronger reduction in pH and an increase in  $f\text{CO}_2$  similar to the trends found in this study. Finally, when evaluating the pH variation and  $\text{CO}_2$  fugacity in the Equatorial Atlantic biome (5°S to 5°N) from 1911 to 2011, it was observed that the reduction in pH and increase in  $f\text{CO}_2$  were close to the trends observed in this study (Lauvset et al., 2015).

In conclusion, the use of empirical models as proposed in this study is an approach that can be successfully used for filling the gap regarding the marine carbonate system in the Western Tropical Atlantic, a region with marked data scarcity.

## Data availability statement

The original contributions presented in the study are included in the article/Supplementary Material. Further inquiries can be directed to the corresponding author.

## Author contributions

CM: Conceptualization, Data curation, Formal analysis, Investigation, Methodology, Writing – original draft, Writing – review & editing. LC: Conceptualization, Formal analysis, Investigation, Methodology, Supervision, Writing – review &

editing. LP: Supervision, Writing – review & editing. AF: Writing – review & editing. MA: Writing – review & editing.

## Acknowledgments

The author(s) declare financial support was received for the research, authorship, and/or publication of this article. We are grateful for the PIRATA program for the installation and maintenance of the mooring site, as well as the availability of online data on salinity, temperature, precipitation and  $f\text{CO}_2$ . We would also like to thank GLODAP for the online availability of TA, DIC and pH data for the region. In addition, we are also thankful for the SOCAT platform for providing the buoy  $f\text{CO}_2$  data. LC (CNPq grant 309708/2021–4, FAPERJ grant E-26/201.156/2022, Prociência/UERJ grant) and MA thank the support of the Brazilian Research Network on Global Climate Change - Rede CLIMA (FINEP-CNPq 437167/2016–0), and the Amazon Coastal Observatory (OCA). We are grateful to Ocean Data View for making freely available the software where the study area maps for this study were made. This study was funded in part by the Coordenação de Aperfeiçoamento de Pessoal de Nível Superior - Brasil (CAPES) - Finance Code 001. CM acknowledges CAPES M.Sc. grant no. 88882.450349/2019–01. This is a contribution to the International Joint Laboratory TAPIOCA (IRD and CAPES/MEC), to the TRIATLAS project, which has received funding from the European Union's Horizon 2020 research and innovation program under grant agreement No 817578, and to the Brazilian Ocean Acidification Research Network – BrOA.

## Conflict of interest

The authors declare that the research was conducted in the absence of any commercial or financial relationships that could be construed as a potential conflict of interest.

## Publisher's note

All claims expressed in this article are solely those of the authors and do not necessarily represent those of their affiliated organizations, or those of the publisher, the editors and the reviewers. Any product that may be evaluated in this article, or claim that may be made by its manufacturer, is not guaranteed or endorsed by the publisher.

## Supplementary material

The Supplementary Material for this article can be found online at: <https://www.frontiersin.org/articles/10.3389/fmars.2024.1286960/full#supplementary-material>

### SUPPLEMENTARY MATERIAL 1

Time series of: (A) Sea Surface Salinity (SSS) and (B) Sea Surface Temperature (SST). Blue dots represent all data available for the period at the buoy and red triangles represent the daily means of the data.

## References

- A'Hearn, P. N., Freitag, H. P., and McPhaden, M. J. (2002). *ATLAS module temperature bias due to solar heating* Vol. 28 Springfield, VA. (NOAA Technical Memorandum OAR PMEL-1). Available at: <https://permanent.fdlp.gov/websites/www.pmel.noaa.gov/pdf-archive/ahca2486.pdf>.
- Allen, R., Foggo, A., Fabricius, K., Balistreri, A., and Hall-Spencer, J. M. (2017). Tropical CO<sub>2</sub> seeps reveal the impact of ocean acidification on coral reef invertebrate recruitment. *Mar. Pollut. Bull.* 124, 607–613. doi: 10.1016/j.marpolbul.2016.12.031
- Allen, M. R., Frame, D. J., Huntingford, C., Jones, C. D., Lowe, J. A., Meinshausen, M., et al. (2009). Warming caused by cumulative carbon emissions towards the trillionth tonne. *Nature* 458, 1163–1166. doi: 10.1038/nature08019
- Araujo, M., Noriega, C., Hounsou-gbo, G. A., Veleda, D., Araujo, J., Bruto, L., et al. (2017). A synoptic assessment of the amazon river-ocean continuum during boreal autumn: from physics to plankton communities and carbon flux. *Front. Microbiol.* 8. doi: 10.3389/fmicb.2017.01358
- Araujo, M., Noriega, C., Medeiros, C., Lefèvre, N., Ibánhez, J. S. P., Flores, M., et al. (2019). On the variability in the CO<sub>2</sub> system and water productivity in the western tropical Atlantic off North and Northeast Brazil. *J. Mar. Syst.* 189, 62–77. doi: 10.1016/j.jmarsys.2018.09.008
- Ashton, I. G., Shutler, J. D., Land, P. E., Woolf, D. K., and Quartly, G. D. (2016). A sensitivity analysis of the impact of rain on regional and global sea-air fluxes of CO<sub>2</sub>. *PLoS One* 11, e0161105. doi: 10.1371/journal.pone.0161105
- Astor, Y. M., Lorenzoni, L., Guzman, L., Fuentes, G., Muller-Karger, F., Varela, R., et al. (2017). Distribution and variability of the dissolved inorganic carbon system in the Cariaco Basin, Venezuela. *Mar. Chem.* 195, 15–26. doi: 10.1016/j.marchem.2017.08.004
- Astor, Y. M., Lorenzoni, L., Thunell, R., Varela, R., Muller-Karger, F., Troccoli, L., et al. (2013). Interannual variability in sea surface temperature and fCO<sub>2</sub> changes in the Cariaco Basin. *Deep Sea Res. Part II: Topical Stud. Oceanogr.* 93, 33–43. doi: 10.1016/j.dsr2.2013.01.002
- Astor, Y. M., Scranton, M. I., Muller-Karger, F., Bohrer, R., and García, J. (2005). fCO<sub>2</sub> variability at the CARIACO tropical coastal upwelling time series station. *Mar. Chem.* 97, 245–261. doi: 10.1016/j.marchem.2005.04.001
- Baker, H. S., Millar, R. J., Karoly, D. J., Beyerle, U., Guillod, B. P., Mitchell, D., et al. (2018). Higher CO<sub>2</sub> concentrations increase extreme event risk in a 1.5°C world. *Nat. Climate Change* 8, 604–608. doi: 10.1038/s41558-018-0190-1
- Bakker, D. C. E., Pfeil, B., Landa, C. S., Metzl, N., O'Brien, K. M., Olsen, A., et al. (2016). A multi-decade record of high-quality fCO<sub>2</sub> data in version 3 of the Surface Ocean CO<sub>2</sub> Atlas (SOCAT). *Earth System Sci. Data* 8, 383–413. doi: 10.5194/essd-8-383-2016
- Bates, N. R., Astor, Y. M., Church, M. J., Currie, K., Dore, J. E., González-Dávila, M., et al. (2014). A time-series view of changing surface ocean chemistry due to ocean uptake of anthropogenic CO<sub>2</sub> and ocean acidification. *Oceanography* 27, 126–141. doi: 10.5670/oceanog.2014.16
- Bates, N. R., and Johnson, R. J. (2020). Acceleration of ocean warming, salinification, deoxygenation and acidification in the surface subtropical North Atlantic Ocean. *Commun. Earth Environ.* 1, 33. doi: 10.1038/s43247-020-00030-5
- Bednaršek, N., Feely, R. A., Howes, E. L., Hunt, B. P. V., Kessouri, F., León, P., et al. (2019). Systematic review and meta-analysis toward synthesis of thresholds of ocean acidification impacts on calcifying pteropods and interactions with warming. *Front. Mar. Sci.* 6. doi: 10.3389/fmars.2019.00227
- Bignami, S., Sponaugle, S., and Cowen, R. K. (2013). Response to ocean acidification in larvae of a large tropical marine fish, *Rachycentron canadum*. *Global Change Biol.* 19, 996–1006. doi: 10.1111/gcb.12133
- Bonou, F., Medeiros, C., Noriega, C., Araujo, M., Hounsou-Gbo, A., and Lefèvre, N. (2022). A comparative study of total alkalinity and total inorganic carbon near tropical Atlantic coastal regions. *J. Coast. Conserv.* 26, 31. doi: 10.1007/s11852-022-00872-5
- Bonou, F. K., Noriega, C., Lefèvre, N., and Araujo, M. (2016). Distribution of CO<sub>2</sub> parameters in the western tropical atlantic ocean. *Dynamics Atmospheres Oceans* 73, 47–60. doi: 10.1016/j.dynatmoce.2015.12.001
- Bourlès, B., Araujo, M., McPhaden, M. J., Brandt, P., Foltz, G. R., Lumpkin, R., et al. (2019). PIRATA: A sustained observing system for tropical atlantic climate research and forecasting. *Earth Space Sci.* 6, 577–616. doi: 10.1029/2018EA000428
- Boyer, T. P. (2005). Linear trends in salinity for the World Ocean 1955–1998. *Geophysical Res. Lett.* 32, L01604. doi: 10.1029/2004GL021791
- Bruto, L., Araujo, M., Noriega, C., Veleda, D., and Lefèvre, N. (2017). Variability of CO<sub>2</sub> fugacity at the western edge of the tropical Atlantic Ocean from the 8°N to 38°W PIRATA buoy. *Dynamics Atmospheres Oceans* 78, 1–13. doi: 10.1016/j.dynatmoce.2017.01.003
- Buapet, P., Gullström, M., and Björk, M. (2013). Photosynthetic activity of seagrasses and macroalgae in temperate shallow waters can alter seawater pH and total inorganic carbon content at the scale of a coastal embayment. *Mar. Freshw. Res.* 64, 1040–1048. doi: 10.1071/MF12124
- Byrne, M. P., Pendergrass, A. G., Rapp, A. D., and Wodzicki, K. R. (2018). Response of the intertropical convergence zone to climate change: location, width, and strength. *Curr. Clim Change Rep.* 4, 355–370. doi: 10.1007/s40641-018-0110-5
- Cai, W.-J., Xu, Y.-Y., Feely, R. A., Wanninkhof, R., Jönsson, B., Alin, S. R., et al. (2020). Controls on surface water carbonate chemistry along North American ocean margins. *Nat. Commun.* 11, 2691. doi: 10.1038/s41467-020-16530-z
- Chen, J. L., Wilson, C. R., and Tapley, B. D. (2010). The 2009 exceptional Amazon flood and interannual terrestrial water storage change observed by GRACE. *Water Resour. Res.* 46. doi: 10.1029/2010WR009383
- Cooley, S. R., Coles, V. J., Subramaniam, A., and Yager, P. L. (2007). Seasonal variations in the Amazon plume-related atmospheric carbon sink. *Global Biogeochem. Cycles* 21, GB3014. doi: 10.1029/2006GB002831
- De Boyer Montégut, C., Madec, G., Fischer, A. S., Lazar, A., and Iudicone, D. (2004). Mixed layer depth over the global ocean: An examination of profile data and a profile-based climatology. *J. Geophys. Res.* 109, 2004JC002378. doi: 10.1029/2004JC002378
- de Carvalho-Borges, M., Orselli, I. B. M., de Carvalho Ferreira, M. L., and Kerr, R. (2018). Seawater acidification and anthropogenic carbon distribution on the continental shelf and slope of the western South Atlantic Ocean. *J. Mar. Syst.* 187, 62–81. doi: 10.1016/j.jmarsys.2018.06.008
- Deser, C., Phillips, A. S., and Alexander, M. A. (2010). Twentieth century tropical sea surface temperature trends revisited. *Geophysical Res. Lett.* 37, L10701. doi: 10.1029/2010GL043321
- Dickson, A. G. (1981). An exact definition of total alkalinity and a procedure for the estimation of alkalinity and total inorganic carbon from titration data. *Deep-Sea Res. Part A-Oceanographic Res. Pap.* 28, 609–623. doi: 10.1016/0198-0149(81)90121-7
- Dickson, A. G. (1990). Standard potential of the reaction: AgCl(s) + 1/2H<sub>2</sub>(g) = Ag(s) + HCl(aq), and the standard acidity constant of the ion HSO<sub>4</sub><sup>-</sup> in synthetic sea water from 273.15 to 318.15 K. *J. Chem. Thermodynamics* 22, 113–127. doi: 10.1016/0021-9614(90)90074-Z
- Dickson, A. G., Sabine, C. L., and Christian, J. R. (eds) (2007). *Guide to Best Practices for Ocean CO<sub>2</sub> measurements. PICES Special Publication, Guide to Best Practices for Ocean CO<sub>2</sub> measurements* (PICES Special Publication). doi: 10.25607/OBP-1342
- Doney, S. C., Fabry, V. J., Feely, R. A., and Kleypas, J. A. (2009). Ocean acidification: the other CO<sub>2</sub> problem. *Annu. Rev. Mar. Sci.* 1, 169–192. doi: 10.1146/annurev.marine.010908.163834
- Dugdale, R. C., Wischmeyer, A. G., Wilkerson, F. P., Barber, R. T., Chai, F., Jiang, M.-S., et al. (2002). Meridional asymmetry of source nutrients to the equatorial Pacific upwelling ecosystem and its potential impact on ocean-atmosphere CO<sub>2</sub> flux; a data and modeling approach. *Deep Sea Res. Part II: Topical Stud. Oceanogr.* 49, 2513–2531. doi: 10.1016/S0967-0645(02)00046-2
- Emerson, S., and Hedges, J. (2008). *Chemical Oceanography and the Marine Carbon cycle* (Cambridge: Cambridge University Press). doi: 10.1017/CBO9780511793202
- Fassbender, A. J., Alin, S. R., Feely, R. A., Sutton, A. J., Newton, J. A., and Byrne, R. H. (2017). Estimating total alkalinity in the Washington state coastal zone: complexities and surprising utility for ocean acidification research. *Estuaries Coasts* 40, 404–418. doi: 10.1007/s12237-016-0168-z
- Field, A. (2007). Amazon and orinoco river plumes and NBC rings: bystanders or participants in hurricane events? *J. Climate* 20, 316–333. doi: 10.1175/JCLI3985.1
- Foltz, G. R., Brandt, P., Richter, I., Rodríguez-Fonseca, B., Hernandez, F., Dengler, M., et al. (2019). The tropical atlantic observing system. *Front. Mar. Sci.* 6. doi: 10.3389/fmars.2019.00206
- Foltz, G. R., McPhaden, M. J., and Lumpkin, R. (2012). A strong atlantic meridional mode event in 2009: the role of mixed layer dynamics\*. *J. Climate* 25, 363–380. doi: 10.1175/JCLI-D-11-00150.1
- Freitag, H. P., Mccarty, M. E., Nosse, C., Lukas, R., Mcphaden, M. J., Cronin, M. F., et al. (1999). *COARE Seacat data: Calibrations and quality control procedures* (Springfield, VA: NOAA Technical Memorandum ERL PMEL-1), 1–93.
- Freitag, H. P., Sawatzky, T. A., Ronnholm, K. B., and J, M. M. (2005). *Calibration procedures and instrumental accuracy estimates of next generation ATLAS water temperature and pressure measurements* (Springfield, VA: NOAA Technical Memorandum OAR PMEL-1).
- Friedlingstein, P., Jones, M. W., O'Sullivan, M., Andrew, R. M., Bakker, D. C. E., Hauck, J., et al. (2022). Global carbon budget 2021. *Earth Syst. Sci. Data* 14, 1917–2005. doi: 10.5194/essd-14-1917-2022
- Friedman, A. R., Reverdin, G., Khodri, M., and Gastineau, G. (2017). A new record of Atlantic sea surface salinity from 1896 to 2013 reveals the signatures of climate variability and long-term trends. *Geophysical Res. Lett.* 44, 1866–1876. doi: 10.1002/2017GL072582
- Friis, K., Körtzinger, A., and Wallace, D. W. R. (2003). The salinity normalization of marine inorganic carbon chemistry data. *Geophysical Res. Lett.* 30, 2002GL015898. doi: 10.1029/2002GL015898
- Goodwin, P., and Lenton, T. M. (2009). Quantifying the feedback between ocean heating and CO<sub>2</sub> solubility as an equivalent carbon emission. *Geophysical Res. Lett.* 36, L15609. doi: 10.1029/2009GL039247
- Gouretski, V. V., and Koltermann, K. P. (2004). *WOCE Global Hydrographic Climatology A Technical Report (No. 35/2004)* (Bundesamt für Seeschifffahrt und Hydrographie).

- Grodsky, S. A., Reul, N., Lagerloef, G., Reverdin, G., Carton, J. A., Chapron, B., et al. (2012). Haline hurricane wake in the Amazon/Orinoco plume: AQUARIUS/SACD and SMOS observations. *Geophysical Res. Lett.* 39, 2012GL053335. doi: 10.1029/2012GL053335
- Grodsky, S. A., Reverdin, G., Carton, J. A., and Coles, V. J. (2014). Year-to-year salinity changes in the Amazon plume: Contrasting 2011 and 2012 Aquarius/SACD and SMOS satellite data. *Remote Sens. Environ.* 140, 14–22. doi: 10.1016/j.rse.2013.08.033
- Guinotte, J. M., and Fabry, V. J. (2008). Ocean acidification and its potential effects on marine ecosystems. *Ann. New York Acad. Sci.* 1134, 320–342. doi: 10.1196/annals.1439.013
- Humphreys, M. P., Lewis, E. R., Sharp, J. D., and Pierrot, D. (2022). PyCO2SYS v1.8: marine carbonate system calculations in Python. *Geosci. Model. Dev.* 15, 15–43. doi: 10.5194/gmd-15-15-2022
- Jiang, Z.-P., Tyrrell, T., Hydes, D. J., Dai, M., and Hartman, S. E. (2014). Variability of alkalinity and the alkalinity-salinity relationship in the tropical and subtropical surface ocean. *Global Biogeochemical Cycles* 28, 729–742. doi: 10.1002/2013GB004678
- Körtzinger, A. (2003). A significant CO<sub>2</sub> sink in the tropical Atlantic Ocean associated with the Amazon River plume. *Geophysical Res. Lett.* 30, 2–5. doi: 10.1029/2003GL018841
- Kroeker, K. J., Kordas, R. L., Crim, R. N., and Singh, G. G. (2010). Meta-analysis reveals negative yet variable effects of ocean acidification on marine organisms. *Ecol. Lett.* 13, 1419–1434. doi: 10.1111/j.1461-0248.2010.01518.x
- Lauvset, S. K., Gruber, N., Landschützer, P., Olsen, A., and Tjiputra, J. (2015). Trends and drivers in global surface ocean pH over the past 3 decades. *Biogeosciences* 12, 1285–1298. doi: 10.5194/bg-12-1285-2015
- Lauvset, S. K., Lange, N., Tanhua, T., Bittig, H. C., Olsen, A., Kozyr, A., et al. (2022). GLODAPv2.2022: the latest version of the global interior ocean biogeochemical data product. *Earth Syst. Sci. Data* 14, 5543–5572. doi: 10.5194/essd-14-5543-2022
- Lee, K., Tong, L. T., Millero, F. J., Sabine, C. L., Dickson, A. G., Goyet, C., et al. (2006). Global relationships of total alkalinity with salinity and temperature in surface waters of the world's oceans. *Geophysical Res. Lett.* 33, 1–5. doi: 10.1029/2006GL027207
- Lefèvre, N., Diverrès, D., and Gallois, F. (2010). Origin of CO<sub>2</sub> undersaturation in the western tropical Atlantic. *Tellus B: Chem. Phys. Meteorol.* 62, 595–607. doi: 10.1111/j.1600-0889.2010.00475.x
- Lefèvre, N., Guillot, A., Beaumont, L., and Danguy, T. (2008). Variability of fCO<sub>2</sub> in the Eastern Tropical Atlantic from a moored buoy. *J. Geophysical Res.: Oceans* 113, 1–12. doi: 10.1029/2007JC004146
- Lefèvre, N., Montes, M. F., Gaspar, F. L., Rocha, C., Jiang, S., De Araújo, M. C., et al. (2017). Net heterotrophy in the Amazon continental shelf changes rapidly to a sink of CO<sub>2</sub> in the outer Amazon plume. *Front. Mar. Sci.* 4. doi: 10.3389/fmars.2017.00278
- Lefèvre, N., Urbano, D. F., Gallois, F., and Diverrès, D. (2014). Impact of physical processes on the seasonal distribution of the fugacity of CO<sub>2</sub> in the western tropical Atlantic. *J. Geophysical Res.: Oceans* 119, 646–663. doi: 10.1002/2013JC009248
- Mahadevan, A., Tagliabue, A., Bopp, L., Lenton, A., Mémerly, L., and Lévy, M. (2011). Impact of episodic vertical fluxes on sea surface pCO<sub>2</sub>. *Philos. Trans. R. Soc. A: Mathematical Phys. Eng. Sci.* 369, 2009–2025. doi: 10.1098/rsta.2010.0340
- Mangi, S. C., Lee, J., Pinnegar, J. K., Law, R. J., Tylilianakis, E., and Birchenough, S. N. R. (2018). The economic impacts of ocean acidification on shellfish fisheries and aquaculture in the United Kingdom. *Environ. Sci. Policy* 86, 95–105. doi: 10.1016/j.envsci.2018.05.008
- Mardani, A., Streimikiene, D., Cavallaro, F., Loganathan, N., and Khoshnoudi, M. (2019). Carbon dioxide (CO<sub>2</sub>) emissions and economic growth: A systematic review of two decades of research from 1995 to 2017. *Sci. Total Environ.* 649, 31–49. doi: 10.1016/j.scitotenv.2018.08.229
- Marengo, J. A., and Espinoza, J. C. (2016). Extreme seasonal droughts and floods in Amazonia: causes, trends and impacts. *Int. J. Climatol.* 36, 1033–1050. doi: 10.1002/joc.4420
- Marion, G. M., Millero, F. J., Camões, M. F., Spitzer, P., Feistel, R., and Chen, C. T. A. (2011). PH of seawater. *Mar. Chem.* 126, 89–96. doi: 10.1016/j.marchem.2011.04.002
- McGillis, W. R., Edson, J. B., Zappa, C. J., Ware, J. D., McKenna, S. P., Terray, E. A., et al. (2004). Air-sea CO<sub>2</sub> exchange in the equatorial Pacific. *J. Geophysical Res.: Oceans* 109, C08S02. doi: 10.1029/2003JC002256
- Merlivat, L., Boutin, J., and Antoine, D. (2015). Roles of biological and physical processes in driving seasonal air-sea CO<sub>2</sub> flux in the Southern Ocean: New insights from CARIOCA pCO<sub>2</sub>. *J. Mar. Syst.* 147, 9–20. doi: 10.1016/j.jmarsys.2014.04.015
- Middelburg, J. J., Soetaert, K., and Hagens, M. (2020). Ocean alkalinity, buffering and biogeochemical processes. *Rev. Geophys.* 58, 1–43. doi: 10.1029/2019RG000681
- Millero, F. J., Graham, T. B., Huang, F., Bustos-Serrano, H., and Pierrot, D. (2006). Dissociation constants of carbonic acid in seawater as a function of salinity and temperature. *Mar. Chem.* 100, 80–94. doi: 10.1016/j.marchem.2005.12.001
- Miot, H. A. (2017). Avaliação da normalidade dos dados em estudos clínicos e experimentais. *Jornal Vasc. Brasileiro* 16, 88–91. doi: 10.1590/1677-5449.041117
- Mitchell, T. P., and Wallace, J. M. (1992). The annual cycle in equatorial convection and sea surface temperature. *J. Climate* 5, 1140–1156. doi: 10.1175/1520-0442(1992)005<1140:TACIEC>2.0.CO;2
- Monteiro, T., Batista, M., Henley, S., da Costa Machado, E., Araujo, M., and Kerr, R. (2022). Contrasting sea-air CO<sub>2</sub> exchanges in the western Tropical Atlantic Ocean. *Global Biogeochemical Cycles* 36, e2022GB007385. doi: 10.1029/2022GB007385
- Muller-Karger, F., Varela, R., Thunell, R., Scranton, M., Bohrer, R., Taylor, G., et al. (2001). Annual cycle of primary production in the Cariaco Basin: Response to upwelling and implications for vertical export. *J. Geophysical Res.: Oceans* 106, 4527–4542. doi: 10.1029/1999JC000291
- Pörtner, H. (2008). Ecosystem effects of ocean acidification in times of ocean warming: a physiologist's view. *Mar. Ecol. Prog. Ser.* 373, 203–217. doi: 10.3354/meps07768
- Razali, N. M., and Wah, Y. B. (2011). Power comparisons of Shapiro-Wilk, Kolmogorov-Smirnov, Lilliefors and Anderson-Darling tests. *J. Stat. Modeling Analytics* 2, 21–33.
- Richey, J. E., Nobre, C., and Deser, C. (1989). Amazon river discharge and climate variability: 1903 to 1985. *Science* 246, 101–103. doi: 10.1126/science.246.4926.101
- Sabine, C. L., Feely, R. A., Gruber, N., Key, R. M., Lee, K., Bullister, J. L., et al. (2004). The oceanic sink for anthropogenic CO<sub>2</sub>. *Science* 305, 367–371. doi: 10.1126/science.1097403
- Santana-Casiano, J. M., González-Dávila, M., Rueda, M.-J., Llinás, O., and González-Dávila, E.-F. (2007). The interannual variability of oceanic CO<sub>2</sub> parameters in the northeast Atlantic subtropical gyre at the ESTOC site. *Global Biogeochemical Cycles* 21, 1–16. doi: 10.1029/2006GB002788
- Schneider, A., Wallace, D. W. R., and Körtzinger, A. (2007). Alkalinity of the Mediterranean Sea. *Geophysical Res. Lett.* 34, 1–5. doi: 10.1029/2006GL028842
- Schuster, U., McKinley, G. A., Bates, N., Chevallier, F., Doney, S. C., Fay, A. R., et al. (2013). An assessment of the Atlantic and Arctic sea-air CO<sub>2</sub> fluxes 1990–2009. *Biogeosciences* 10, 607–627. doi: 10.5194/bg-10-607-2013
- Serra, Y. L., A'Hearn, P., Freitag, H. P., and McPhaden, M. J. (2001). ATLAS self-siphoning rain gauge error estimates. *J. Atmospheric Oceanic Technol.* 18, 1989–2002. doi: 10.1175/1520-0426(2001)018<1989:ASSRGE>2.0.CO;2
- Silva, A. C., Araujo, M., and Bourlès, B. (2010). Seasonal variability of the Amazon river plume during revizee program. *Trop. Oceanogr.* 38, 76–87. doi: 10.5914/tropocean.v38i1
- Sunda, W. G., and Cai, W. (2012). Eutrophication induced CO<sub>2</sub>-acidification of subsurface coastal waters: interactive effects of temperature, salinity, and atmospheric P CO<sub>2</sub>. *Environ. Sci. Technol.* 46, 10651–10659. doi: 10.1021/es300626f
- Sutton, A. J., Battisti, R., Carter, B., Evans, W., Newton, J., Alin, S., et al. (2022). Advancing best practices for assessing trends of ocean acidification time series. *Front. Mar. Sci.* 9. doi: 10.3389/fmars.2022.1045667
- Takahashi, T., Sutherland, S. C., Sweeney, C., Poisson, A., Metz, N., Tilbrook, B., et al. (2002). Global sea-air CO<sub>2</sub> flux based on climatological surface ocean pCO<sub>2</sub>, and seasonal biological and temperature effects. *Deep Sea Res. Part II: Topical Stud. Oceanogr.* 49, 1601–1622. doi: 10.1016/S0967-0645(02)00003-6
- Takahashi, T., Sutherland, S. C., Wanninkhof, R., Sweeney, C., Feely, R. A., Chipman, D. W., et al. (2009). Climatological mean and decadal change in surface ocean pCO<sub>2</sub>, and net sea-air CO<sub>2</sub> flux over the global oceans. *Deep Sea Res. Part II: Topical Stud. Oceanogr.* 56, 554–577. doi: 10.1016/j.dsr2.2008.12.009
- Ternon, J. F., Oudot, C., Dessier, A., and Diverres, D. (2000). A seasonal tropical sink for atmospheric CO<sub>2</sub> in the Atlantic ocean: the role of the Amazon River discharge. *Mar. Chem.* 68, 183–201. doi: 10.1016/S0304-4203(99)00077-8
- Wallace, R. B., Baumann, H., Grear, J. S., Aller, R. C., and Gobler, C. J. (2014). Coastal ocean acidification: The other eutrophication problem. *Estuarine Coast. Shelf Sci.* 148, 1–13. doi: 10.1016/j.ecss.2014.05.027
- Wolf-Gladrow, D. A., Zeebe, R. E., Klaas, C., Körtzinger, A., and Dickson, A. G. (2007). Total alkalinity: The explicit conservative expression and its application to biogeochemical processes. *Mar. Chem.* 106, 287–300. doi: 10.1016/j.marchem.2007.01.006
- Xue, L., and Cai, W.-J. (2020). Total alkalinity minus dissolved inorganic carbon as a proxy for deciphering ocean acidification mechanisms. *Mar. Chem.* 222, 103791. doi: 10.1016/j.marchem.2020.103791